

The 125 GeV Higgs signal at the LHC in the CP-violating MSSM

Amit Chakraborty^a, Biswaranjan Das^b, J. Lorenzo Diaz-Cruz^c, Dilip Kumar Ghosh^a,
Stefano Moretti^d and Poulouse Poulouse^b

^a *Department of Theoretical Physics, Indian Association for the Cultivation of Science,
2A & 2B, Raja S.C. Mullick Road, Jadavpur, Kolkata 700 032, India.*

^b *Department of Physics,
IIT Guwahati, Assam 781039, India.*

^c *Facultad de Ciencias Físico-Matemáticas,
Benemérita Universidad Autónoma de Puebla, Puebla, México*

^d *School of Physics & Astronomy,
University of Southampton, Highfield, Southampton SO17 1BJ, UK.*

Abstract

The ATLAS and CMS collaborations have observed independently at the Large Hadron Collider (LHC) a new Higgs-like particle with a mass $M_h \sim 125$ GeV and properties similar to that predicted by the Standard Model (SM). Although the measurements indicate that this Higgs-like boson is compatible with the SM hypothesis, however due to large uncertainties in some of the Higgs detection channels, one still has the possibility of testing this object as being a candidate for some Beyond the SM (BSM) physics scenarios, for example, the Minimal Supersymmetric Standard Model (MSSM), in the CP-conserving version (CPC-MSSM). In this paper, we evaluate the modifications of these CPC-MSSM results when CP-violating (CPV) phases are turned on explicitly, leading to the CP-violating MSSM (CPV-MSSM). We investigate the role of the CPV phases in (some of) the soft Supersymmetry (SUSY) terms on both the mass of the lightest Higgs boson h_1 , and the rates for the processes $gg \rightarrow h_1 \rightarrow \gamma\gamma$, $gg \rightarrow h_1 \rightarrow ZZ^* \rightarrow 4l$, $gg \rightarrow h_1 \rightarrow WW^* \rightarrow l\nu l\nu$, $pp \rightarrow Vh_1 \rightarrow Vb\bar{b}$ and $pp \rightarrow Vh_1 \rightarrow V\tau^+\tau^-$, ($V \equiv W^\pm, Z$) at the LHC, considering the impact of the flavor constraints as well as the constraints coming from the Electric Dipole Moment (EDM) measurements. We find that it is possible to have a Higgs mass of about 125 GeV with relatively small $\tan\beta$, large A_t and a light stop, which is consistent with the current SUSY particle searches at the LHC. We obtain that the imaginary part of the top and bottom Yukawa couplings can take very small but non-zero values even after satisfying the recent updates from both the ATLAS and CMS collaborations within $1-2\sigma$ uncertainties which might be an interesting signature to look for at the future run of the LHC. Our study shows that the CPV-MSSM provides an equally potential solution (like its CP-conserving (CPC) counterpart) to the recent LHC Higgs data, in fact offering very little in the way of distinction

between these two SUSY models (CPC-MSSM and CPV-MSSM) at the 7 and 8 TeV run of the LHC. Improvement in different Higgs coupling measurements is necessary in order to test the possibility of probing the small dependence on these CPV phases in the Higgs sector of the MSSM.

E-mail: tpac@iacs.res.in, biswaranjan@iitg.ernet.in, jldiaz@fcfm.buap.mx, tpdkg@iacs.res.in,
S.Moretti@soton.ac.uk, poulose@iitg.ernet.in

1 Introduction

The experimental observation of the SM Higgs boson and the determination of its properties were among the main motivations behind the construction of the LHC. Both the ATLAS and CMS collaborations reported a Higgs boson discovery with the new particle having mass around 125 GeV [1–4]. It is also evident from the results that the observed signals in the different production and decay channels available seem to follow the SM predictions. However, primarily due to the presence of large experimental uncertainties, there could be some deviations in some of the individual channels from the SM expectations. According to the recent updates on LHC results, CMS results are consistent with the SM expectations within 1σ uncertainty in all channels, except for a slight tension in the case of $h \rightarrow WW^*$ [5–10]. On the other hand, a slight excess still persists in the case of ATLAS observations in most of the channels [11–17]. While not incompatible with statistical fluctuations, it is also possible that such deviations could signal the presence of BSM physics. For instance, one can explain these results in models with an extended Higgs sector like those embedded in SUSY [18–21].

SUSY is in fact one of the most popular extensions of the SM, with motivations that include: i) the solution to the hierarchy and naturalness problems of the SM; ii) the unification of the SM gauge couplings at some high scale close to the Planck mass; iii) the provision of a Dark Matter (DM) candidate (so long that R -parity conservation is postulated); iv) being a natural ingredient of String theories.

The MSSM though, the simplest realization of SUSY, predicts the maximum tree-level value of the lightest Higgs mass to be $M_h \leq M_Z$. Significant radiative corrections are needed in order to push M_h beyond the latest LEP bound, $M_h > 114$ GeV. However, making the Higgs mass close to 125 GeV requires the inclusion of sizable top/stop loop corrections, which depend quadratically on the top quark mass and logarithmically on the stop masses, combined with a large value of $\tan\beta$, the ratio of the Vacuum Expectation Values (VEVs) of the two Higgs doublets pertaining to the MSSM. Several studies have already been performed in the context of different SUSY models, including the MSSM [22–42] (also the constrained version [43]), NMSSM [44] and (B–L)SSM [45]. All of these scenarios predict a SM-like Higgs boson with mass around 125 GeV and also offer solutions explaining the potential slight disagreement between the data and the SM predictions in different decay channels.

Another route to follow in order to obtain similar results is to consider the possibility of having non-zero values of the CPV phases in (some of) the soft SUSY parameters that can substantially modify Higgs boson phenomenology at colliders at both mass spectrum and production/decay level. This motivated an avalanche of phenomenological studies in this CPV-MSSM framework [46–76]. In the presence of CPV complex parameters, the top and bottom squarks couplings to the Higgs state will be modified substantially in a large domain of the MSSM parameter space [77–81]. Conversely

though the CP phases in the MSSM are significantly constrained by the EDM measurements. At the same time, the non-zero phases, satisfying the EDM constraints, may be allowed, as explained in the following sections, and in some details in Refs. [82–88].

The Higgs potential of the MSSM is CP invariant at tree level. Several studies have been performed to break the CP invariance of the Higgs potential spontaneously [89]. However, these possibilities are now almost ruled out by various experiments [90]. Instead, CP violation can be induced explicitly in the Higgs sector of the MSSM. This can be achieved by introducing complex parameters that break CP invariance in the sfermion and chargino/neutralino sectors. There are many new parameters which could in principle be complex and thus possess CPV phases, like the Higgsino mass parameter (μ), the soft SUSY breaking gaugino masses (M_1, M_2, M_3) and the soft trilinear couplings (A_f) of the Higgs boson to the (massive) sfermions of flavor f . In general, each of these phases can be independent. The CPV effects are then carried into the Higgs sector through the interactions of the two Higgs doublets with the sfermions and/or charginos/neutralinos.

In this paper, we will study the possibilities to have the Higgs signals with mass around 125 GeV in the context of such a CPV-MSSM, which are in agreement with the aforementioned LHC data as well as other experimental constraints. We will look for parameter configurations of the model for which there exists agreement with both the Higgs mass and the rates into the channels observed by the LHC. We will investigate the dependence of the feasible CPV-MSSM signals on the couplings of the Higgs boson to both the relevant particle and sparticle states entering the model spectrum, as well as upon the masses of the latter, thereby aiming at a general understanding of the role of the complex phases. While scanning the CPV-MSSM parameter space, we also take into account the constraints coming from the flavor sector and the EDM measurements.

The paper is structured as follows. In the next section we give a brief introduction to the Higgs sector of the CPV-MSSM. In Sec. 3 we discuss the relevant experimental constraints coming from the SUSY particle searches, flavor sector and EDM measurements. In Sec. 4 we investigate the possible numerical values of its parameters after performing scans of the CPV-MSSM parameter space against available experimental constraints. In Sec. 5 we present our results on Higgs production and decay processes in connection with the LHC Higgs data. Finally, we conclude in Sec. 6.

2 A light Higgs mass within the CPV-MSSM

Within the framework of the MSSM, non-zero phases of μ , M_i ($i = 1, 2, 3$) and/or A_f ($f = t, b, \tau$) can induce CP violation in the Higgs sector radiatively, via the interactions of the Higgs bosons with the sfermions and gauginos. These interactions lead to modifications of the Higgs masses as well as the Higgs couplings, breaking the CP invariance of the tree level scalar potential. Presence of CP violation in the Higgs sector leads to scalar-pseudoscalar mixing, resulting in CP-mixed physical Higgs states. In the following we describe this mixing schematically and explicitly present

the dependence of mixing on different complex parameters. The gauge eigenstates of the MSSM Higgs doublets are given by

$$\Phi_1 = \begin{pmatrix} \phi_1^+ \\ \phi_1^0 + i\eta_1^0 \end{pmatrix}, \quad \Phi_2 = \begin{pmatrix} \phi_2^0 + i\eta_2^0 \\ \phi_2^- \end{pmatrix}, \quad (1)$$

with

$$\langle \Phi_1^0 \rangle = \frac{1}{\sqrt{2}} \begin{pmatrix} 0 \\ v_u \end{pmatrix}, \quad \langle \Phi_2^0 \rangle = \frac{1}{\sqrt{2}} \begin{pmatrix} v_d \\ 0 \end{pmatrix}$$

and where η_i^0 ($i = 1, 2$) are the pseudoscalar components of the two Higgs doublets.

In the presence of the CPV phases in the scalar potential, the mass matrix for the neutral Higgs bosons enters through the general form

$$\mathcal{L}_{\text{mass}} = \begin{pmatrix} \eta_1^0 & \eta_2^0 & | & \phi_1^0 & \phi_2^0 \end{pmatrix} \left(\begin{array}{c|c} \mathcal{M}_P^2 & \mathcal{M}_{SP}^2 \\ \hline \hline \hline [\mathcal{M}_{SP}^2]^T & \mathcal{M}_S^2 \end{array} \right) \begin{pmatrix} \eta_1^0 \\ \eta_2^0 \\ \phi_1^0 \\ \phi_2^0 \end{pmatrix}. \quad (2)$$

This 4×4 mass matrix is divided into 2×2 blocks with \mathcal{M}_P^2 and \mathcal{M}_S^2 representing the mixing within the pseudoscalar and scalar states, respectively, and the off-diagonal block, \mathcal{M}_{SP}^2 , representing the mixing between the scalar-pseudoscalar states. Note that \mathcal{M}_{SP}^2 is absent in the CPC-MSSM and is generated in the CPV-MSSM through one-loop corrections [91–99]. Different contributions to the terms in the 2×2 matrix \mathcal{M}_{SP}^2 can be summarized as follows [91, 92]:

$$\mathcal{M}_{SP}^2 \approx \mathcal{O} \left(\frac{M_t^4 |\mu| |A_t|}{v^2 32\pi^2 M_{\text{SUSY}}^2} \right) \sin \Phi_{\text{CP}} \times \left[6, \frac{|A_t|^2}{M_{\text{SUSY}}^2}, \frac{|\mu|^2}{\tan \beta M_{\text{SUSY}}^2}, \frac{\sin 2\Phi_{\text{CP}} |A_t| |\mu|}{\sin \Phi_{\text{CP}} M_{\text{SUSY}}^2} \right], \quad (3)$$

where $\Phi_{\text{CP}} = \text{Arg}(A_t \mu)$, $v = 246$ GeV and the mass scale M_{SUSY} is defined by

$$M_{\text{SUSY}}^2 = \frac{m_{\tilde{t}_1}^2 + m_{\tilde{t}_2}^2}{2}, \quad (4)$$

with $m_{\tilde{t}_1}$ and $m_{\tilde{t}_2}$ being the stop masses.

One can easily estimate the degree of CP violation in the Higgs sector by considering the dominant one(s) of these contributions. For example, sizeable scalar-pseudoscalar mixing is possible for a large CPV phase Φ_{CP} , $|\mu|$ and $|A_t| > M_{\text{SUSY}}$. Apart from a massless Goldstone boson G^0 , which does not mix further with the other neutral states, the 4×4 mass matrix effectively reduces to a 3×3 Higgs mass-squared matrix \mathcal{M}^2 , in the basis (A, ϕ_1^0, ϕ_2^0) , where A is the appropriate eigenstate of \mathcal{M}_P^2 . The 3×3 symmetric matrix \mathcal{M}_{ij}^2 can be diagonalized by an orthogonal matrix \mathcal{O} , i.e., $M_i^2 \delta_{ij} = \mathcal{O}_{ik} \mathcal{M}_{kl}^2 \mathcal{O}_{jl}$, leading to physical states, $h_i = \mathcal{O}_{ji} \phi_j$, where $\phi_j \equiv (A, \phi_1^0, \phi_2^0)$. In this article, the physical mass eigenstates h_1, h_2 and h_3 are considered in ascending order of mass ($M_{h_1} < M_{h_2} < M_{h_3}$). Moreover, as A is no longer a physical state, the charged Higgs boson mass

M_{H^\pm} is a more appropriate parameter for the description of the CPV-MSSM Higgs sector instead of M_A often used in the CPC-MSSM. Hence, the tree level Higgs masses in the CPV-MSSM can be conveniently expressed in terms of $\tan\beta$ and M_{H^\pm} .

Radiative corrections enhance the Higgs mass significantly via the top quark Yukawa coupling, the third generation top squark mass parameters M_{Q3} , M_{U3} and the trilinear coupling A_t , while the bottom squark sector has a somewhat subdued effect. At the same time though, flavor physics observations from the b -quark sector often serve as stringent constraints on Higgs phenomenology and we therefore include the sbottom sector parameters M_{D3} and the trilinear coupling A_b along with the above mentioned top squark parameters. The stau sector, in principle, can play a significant role in the Higgs to di-photon decay mode. To take this into account, we include the parameters M_{L3} , M_{E3} and A_τ corresponding to the stau sector in our parameter space scan.

Coming to the first two generations of the soft masses, it is well known that they have very little effect on the Higgs sector of the MSSM. At the same time, their phases $\phi_{A_{e/\mu}}$, $\phi_{A_{u/d}}$ can provide significant contributions to the atomic EDMs. These can however be drastically reduced either by assuming these phases to be sufficiently small or by taking the first and second generation squarks and sleptons sufficiently heavy. This is achieved by setting the hierarchy factor between the first two and third generation soft masses to be 20. Nonetheless, sizeable contributions to the EDMs are always possible from Higgs-mediated two-loop diagrams [100–102]. Therefore, in order to ascertain whether the regions of parameter space of interest here are potentially compatible with the EDM constraints, we have calculated the EDMs of Thallium, Mercury, electron and neutron (d_{Tl} , d_{Hg} , d_e , d_n) and compared the results with the current bounds [85, 103–113]. However, we would like to clarify that in the present analysis, wherein we mainly focus on the possibility of a 125 GeV Higgs boson signal in the CPV-MSSM, we do not perform detailed studies of the different EDMs. In fact, in general, it has been shown in [85] that the constraints from the EDMs are highly dependent upon the combinations of different phases of soft SUSY breaking parameters as different loop diagrams can interfere either destructively or constructively so as to either suppress or enhance, respectively, individual contributions to the EDMs. In the case of d_{Hg} , the experimental limits put severe constraint on ϕ_3 , due to the strong correlation between this phase and $\phi_{A_{u,d}}$, both of which enter the EDM operators at one loop level. In contrast, d_n and d_{Tl} limits have a relatively stronger impact on ϕ_2 though, presently, the latter constraint is not strongly correlated with any of the other phases. A detailed analysis of the impact of the EDM data in the Higgs sector of the CPV-MSSM, considering all the three Higgs bosons and all CPV phases, is complicated and beyond the scope of this study. Nevertheless, herein we take a straightforward approach and present our results after comparing with the available EDM constraints. In the following section we present our numerical analyses and discuss the parameter space within the CPV-MSSM respecting these constraints along with all other experimental restrictions including those from the flavor sector.

3 Current experimental constraints

As explained in Sec. 2, the non-trivial CPV phases modify the Higgs mass significantly by introducing mixing between the scalar and pseudoscalar Higgs sector. CPV phases can also affect the Higgs couplings with the gauge bosons and fermions, altering significantly their tree level values. For example, in a situation with maximal CP violation, known as CPX scenario [66, 97, 114, 115], one can have the lightest Higgs boson which is almost CP-odd with a highly suppressed coupling to a pair of W 's or Z 's [91, 92].

Both the ATLAS and CMS collaborations reported the best fit results of invariant mass in the two high resolution channels, $\gamma\gamma$ and $ZZ^* \rightarrow 4\ell$ ($\ell = e, \mu$) as 125.5 ± 0.2 (stat.) $^{+0.5}_{-0.6}$ (syst.) GeV [4] and 125.3 ± 0.4 (stat.) ± 0.5 (syst.) GeV [3], respectively. Thus, considering the 1σ uncertainty band around the best fit value, we primarily demand that the lightest Higgs boson mass (M_{h_1}) should always lie in the range of 124.0 - 126.0 GeV, while scanning the CPV-MSSM parameter space. Besides this, we also enforce the following constraints to select the final allowed parameter space points for our further analyses.

We impose 95% Confidence Limit (CL)¹ lower bounds on the masses of sparticles, listed by the Particle Data Group (PDG) [116], as follows:

$$\begin{aligned} M_{\tilde{\chi}_1^0} &> 46 \text{ GeV}, & M_{\tilde{\chi}_2^0} &> 62.4 \text{ GeV}, & M_{\tilde{\chi}_1^\pm} &> 94 \text{ GeV}, \\ M_{\tilde{t}_1} &> 95.7 \text{ GeV}, & M_{\tilde{b}_1} &> 89 \text{ GeV}, & M_{\tilde{g}} &> 800 \text{ GeV}. \end{aligned} \quad (5)$$

It is well known that the flavor observables play a crucial role in determining the viable regions of the SUSY parameter space. Several rare b-decays, which are helicity suppressed in the SM, can acquire substantial contribution from different SUSY particles present in the model and these corrections may come with same or opposite sign with the SM expectations. To take into account the stringent constraints on the SUSY parameter space coming from the flavor sector, we consider several low energy processes like the purely leptonic decay of $B_s \rightarrow \mu^+\mu^-$ and $B_d \rightarrow \tau^+\tau^-$, the radiative decay $b \rightarrow s\gamma$ etc. The $B_s \rightarrow \mu^+\mu^-$ decay is a flavor changing neutral current process which occurs at the loop level in both the SM and MSSM. In the SM, it is helicity suppressed by the muon mass, which results in tiny SM expectation for the branching ratio of the order of 10^{-9} [117]. For large values of $\tan\beta$, order of magnitude enhancements of the $Br(B_s \rightarrow \mu^+\mu^-)$ are possible in the MSSM, for details see Ref. [118–120] and the references therein. In the MSSM, the dominant contribution mainly comes from the Higgs penguin diagrams with the exchange of the heavy scalars present in the flavor changing b \rightarrow s couplings. Besides, there are also contributions from the charged Higgs and gluino exchange diagrams which may interfere constructively or destructively with the

¹In our analysis, we consider 3σ bound for almost all the experimental constraints. But, for the sparticle masses, we find 95% CL limit from the Particle Data Group [116]. We check that the updated results on different sparticle masses, which are available in the literature but not yet included in the PDG database, do not change our results substantially.

Higgs diagrams and the SM expectations depending upon the sign of the μ and A_t terms. Due to its strong dependence on $\tan\beta$, MSSM parameter space with large $\tan\beta$ is now highly constrained by the current experimental results on $Br(B_s \rightarrow \mu^+\mu^-)$ [121, 122]. The combined experimental result from the LHCb and CMS for $Br(B_s \rightarrow \mu^+\mu^-)$ is $(2.9 \pm 0.7) \times 10^{-9}$ [123–125] and in our analysis we consider the 3σ error band around the central value,

$$0.8 \times 10^{-9} < Br(B_s \rightarrow \mu^+\mu^-) < 5.0 \times 10^{-9}. \quad (6)$$

Let us now consider another important b-observable, namely $Br(b \rightarrow s\gamma)$. In the SM, it comes from the $t - W$ loop [126] and, in the MSSM, the dominant contribution comes from the $t - H^\pm$ and $\tilde{t}_{1,2} - \tilde{\chi}_{1,2}^\pm$ loops [127], where the former have the same sign with the SM $t - W$ loop. The chargino loop contribution is proportional to the product $A_t\mu\tan\beta$. Depending on the sign of $A_t\mu$, there might be cancellation or enhancement between the above two loop contributions within the MSSM [128]. Here, we choose positive A_t and positive μ and so we expect some cancellation between these different SUSY corrections for large values of $\tan\beta$. Considering the large uncertainty in the measurement of $b \rightarrow s\gamma$, we here assume 3σ uncertainty around the experimental value of $Br(b \rightarrow s\gamma) = (3.43 \pm 0.22) \times 10^{-4}$ [129] which leads to

$$2.77 \times 10^{-4} < Br(b \rightarrow s\gamma) < 4.09 \times 10^{-4}. \quad (7)$$

Apart from the above-mentioned two flavor constraints, which play a significant role in the present study, there exist other flavor constraints with subdued influences. The mass differences measured in the $B_0 - \bar{B}_0$ mixing, ΔM_{B_d} and ΔM_{B_s} , are equally sensitive to the new physics contributions. For both these two observables, at large $\tan\beta$, non-negligible contribution comes from the most dominant double scalar penguin (DP) diagrams [130, 131]. The experimental and the SM values for the mass differences in the B_d system are: $\Delta M_{B_d}^{\text{Exp}} = 0.510 \pm 0.004 \text{ ps}^{-1}$ [116, 129, 132] and $\Delta M_{B_d}^{\text{SM}} = 0.502 \pm 0.006 \text{ ps}^{-1}$ [133], respectively. On the other hand, for the B_s system they are, $\Delta M_{B_s}^{\text{Exp}} = 17.768 \pm 0.024 \text{ ps}^{-1}$ [132, 134] and $\Delta M_{B_s}^{\text{SM}} = 17.3 \pm 2.6 \text{ ps}^{-1}$ [135]. The SUSY contributions to the $B_d^0 - \bar{B}_d^0$ and $B_s^0 - \bar{B}_s^0$ mass differences are usually denoted as $\Delta M_{B_d}^{\text{SUSY}}$ and $\Delta M_{B_s}^{\text{SUSY}}$, respectively and calculated by subtracting the SM prediction from the experimentally measured quantity i.e. $\Delta M_{B_d}^{\text{SUSY}} = \Delta M_{B_d}^{\text{Exp}} - \Delta M_{B_d}^{\text{SM}}$ [136, 137]. Note that, the theoretical uncertainty associated to ΔM_{B_s} dominates the experimental uncertainties, unlike ΔM_{B_d} where both theoretical and experimental error bars are relatively small. In rest of our analysis, we therefore, consider only ΔM_{B_d} mass difference² and allow the SUSY contribution $\Delta M_{B_d}^{\text{SUSY}}$ lie within the 3σ error band drawn around the experimental best-fit number. We also consider the ratio of the experimentally measured $Br(B_u \rightarrow \tau\nu)$ to its SM value, $R_{B_u \rightarrow \tau\nu} = \frac{Br^{\text{Exp}}(B_u \rightarrow \tau\nu)}{Br^{\text{SM}}(B_u \rightarrow \tau\nu)} = 1.21 \pm 0.30$ [120, 138]. Besides, we further check whether our results are consistent with the experimental result on the $Br(B_d \rightarrow \tau^+\tau^-)$ available in the Particle Data Group [116].

²We check that if we consider the ΔM_{B_s} mass difference after satisfying eq.8 and allow even 1σ uncertainty in $\Delta M_{B_s}^{\text{SUSY}}$ estimation, we loose only $\sim 1\%$ points. We plot the correlation of these two observables ($\Delta M_{B_s}^{\text{SUSY}}$ and $\Delta M_{B_d}^{\text{SUSY}}$) in Fig.7(a) and the figure itself justify our claim.

Finally, we consider the measurement of direct CP asymmetry, $A_{\text{CP}}(B \rightarrow X_s \gamma)$ associated with the $B \rightarrow X_s \gamma$ decay with its present limit -0.008 ± 0.029 [116]. So, in summary, the experimental limits used, corresponding to 3σ uncertainty, (except the $Br(B_d \rightarrow \tau^+ \tau^-)$ which is given at 90% CL in the PDG) are the following:

$$0.31 < R_{B_u \rightarrow \tau \nu} < 2.1, \quad Br(B_d \rightarrow \tau^+ \tau^-) < 4.1 \times 10^{-3}, \\ -0.095 < A_{\text{CP}}(B \rightarrow X_s \gamma) < 0.079, \quad -0.0136 < \Delta M_{B_d}^{\text{SUSY}} < 0.0296 \text{ ps}^{-1}. \quad (8)$$

All these constraints are imposed on the points satisfying the primary selection criterion on the Higgs boson mass.

Furthermore, we investigate the effect of the EDM constraints on the parameter space. As already discussed, atomic EDMs receive contributions from d_e , as well as quark EDMs or Chromo EDMs (CEDMs). While in a quantum field theory, like the CPV-MSSM being discussed here, the presence of CPV phases induces EDMs for elementary particles like the electrons and quarks. How these contributions present themselves at the atomic level is a complex phenomenon, which depends on the nature of the atom or molecule being studied and on the theoretical model being considered. In the case of diamagnetic systems like Mercury (Hg), the dominant contribution comes from the CEDMs, while the effect of d_e is sub-dominant. It is known that these atomic EDMs receive large theoretical (hadronic and nuclear) uncertainties arising from the hadronic CPV. Besides, while the EDM of Hg is one of the best known experimentally, theoretical calculations using different techniques do not quite agree with each other, for reasons those are not fully understood [113]. Thus, the upper bounds on d_e obtained from these results should be considered with caution [106, 108]. In contrast, in the case of paramagnetic systems like Thallium (Tl) and Ytterbium Fluoride (YbF), the atomic EDMs depend on d_e and another term arising from electron-nucleon interactions, therefore the d_e extracted from these systems are more reliable. Traditionally, while extracting d_e from these systems, it is assumed that only the single unpaired electron would contribute to their EDMs. Besides, there are also direct measurements on d_n [109, 110], which receives contributions from the CEDMs arising in several BSM models. Similar to the atomic case, these results too receive large theoretical uncertainties. We listed the current bounds on d_n , d_{Tl} and d_{Hg} in Tab.1. At present,

System	Present limit on absolute value
$ d_n $	$3.3 \times 10^{-26} \text{ e cm (95\% CL) [109, 110]}$
$ d_{Tl} $	$9.0 \times 10^{-25} \text{ e cm (90\% CL) [85, 105]}$
$ d_{Hg} $	$3.1 \times 10^{-29} \text{ e cm (95\% CL) [103]}$

Table 1: Summary table for the current experimental limits on d_n , d_{Tl} and d_{Hg} .

the most stringent model independent limit on d_e stem from the searches for the EDMs of YbF and Tl, with upper limits of $1.05 \times 10^{-27} \text{ e cm [104]}$ and $1.6 \times 10^{-27} \text{ e cm [105]}$ at 90% CL, respectively. An improved analysis including the effect of electron-nucleon interaction and combining the results

from Tl, YbF and Hg is available in Ref. [106]. While considering the d_e constraints coming from these experiments, we adopt the result of this analysis with d_e given at 95% CL [106] as

$$|d_e| < 1.4 \times 10^{-27} \text{ e cm.} \quad (9)$$

However, the Advanced Cold Molecule Electron (ACME) EDM Collaboration [107] measurement recently put a strong limit on d_e which is down by one order of magnitude compared to the previous measurements. The experimental bound at 90% CL is:³

$$|d_e| < 8.7 \times 10^{-29} \text{ e cm.} \quad (10)$$

In the next section, we first discuss the details of our CPV-MSSM parameter space scan and then show the impact of these constraints on the CPV-MSSM parameter space.

4 Impact of the constraints on the parameter space

Here we explore the CPV-MSSM parameter space in order to estimate the regions which respect all the above mentioned experimental constraints. The scans were performed using the publicly available numerical package CPsuperH (version 2.3) [139]. We here consider two separate scans with different sets of input parameters.⁴ The choice of the first set of input parameters was aimed at maximizing the effect of CP violation in MSSM, while the second set was with a view at searching for solutions within the CPV-MSSM compatible with the LHC and other experimental results.

4.1 Scan 1: with maximum CPV phases

The first scan considered the following values of the input parameters:

$$\begin{aligned} 1 < \tan \beta < 60, & \quad 100 \text{ GeV} < M_{H^\pm} < 300 \text{ GeV}, \\ 50 \text{ GeV} < |M_1| < 500 \text{ GeV}, & \quad 100 \text{ GeV} < |M_2| < 1000 \text{ GeV}, \\ 500 \text{ GeV} < A_t = A_b = A_\tau < 3000 \text{ GeV}, & \quad 500 \text{ GeV} < |\mu| < 2000 \text{ GeV}, \\ 500 \text{ GeV} < M_{Q3}, M_{U3} < 2000 \text{ GeV}, & \quad 500 \text{ GeV} < M_{D3} < 2000 \text{ GeV}, \\ 100 \text{ GeV} < M_{L3}, M_{E3} < 2000 \text{ GeV}. & \end{aligned} \quad (11)$$

The 100 GeV lower limit for M_2 is taken from the LEP-2 lower bound from model-independent chargino searches, while the lower limit on $\tan \beta$ is close to the LEP-2 Higgs search exclusion. In

³Here we would like to note that there are certain observables for which 90% or 95% CL data are available in the literature, so we consider them at the same CL which are available, for example the sparticle mass bounds at the PDG are given at 95% CL, while some of the EDM results are available either at 90% CL or at 95% CL.

⁴The reader may note that the first set of the parameter space scanning was planned and performed when preliminary results of the LHC were available. However, the second scan is performed keeping in mind the latest results of the LHC and the recent electron EDM measurement by the ACME collaboration.

Ref. [51, 52], it was shown that there is a transition point at $M_{H^\pm} \sim 150$ GeV (for some specific choices of the model parameters) above which the lightest Higgs mass state, h_1 , is almost a pure scalar state and thus there would be no CP violation effect through the scalar and pseudoscalar mixing. So, in our first scan (Scan 1), we set the upper limit on M_{H^\pm} at 300 GeV in accordance with the above observation. However, we will see in Sec. 4.2, interesting phenomenology appears when we relax this upper limit on the H^\pm mass. In order to have maximum CP violation, the three phases ϕ_{A_f} ($f = t, b, \tau$) and ϕ_3 are fixed at 90° , while all other phases are set to zero. Trilinear couplings of the first and second sfermion families ($|A_e|, |A_\mu|, |A_u|, |A_d|, |A_c|, |A_s|$) are less relevant for our analysis, hence we have set them to zero. Both the CMS and ATLAS collaborations have already excluded gluino masses less than 1.1 TeV for different possible final states in the context of the Constrained-MSSM (CMSSM) [140, 141]. Note that, the CMSSM bound can not be directly applied here as the bound is expected to change in the context of the CPV-MSSM due to modifications in the different decay/branching ratios. Here, we fix the magnitude and phase of the gluino mass parameter M_3 at 1.2 TeV and 90° respectively just to reduce the number of free parameters.

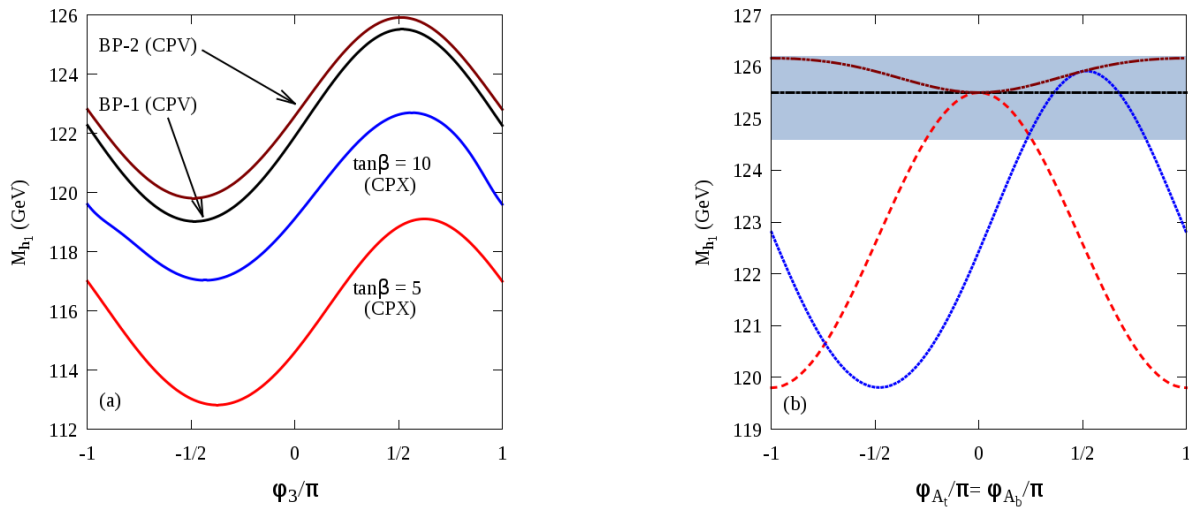


Figure 1: In panel (a) we show the dependence of M_{h_1} upon ϕ_3 for two BPs from our scan (upper two curves) against two benchmark points in the CPX scenario (lower two curves), keeping $\phi_{A_t} = \phi_{A_b} = \pi/2$. While in panel (b) the red (dash-dotted), blue (small dash) and brown (long-dash dotted) curves correspond to $\phi_3 = 0$, $\phi_3 = \pi/2$, and $\phi_{A_t} = \phi_{A_b} = \phi_3$, respectively, corresponding to BP-2. The horizontal solid curve in panel (b) represents the value of M_{h_1} in the CPC-MSSM and the shaded region corresponds to the 1σ range of the observed Higgs boson mass 125.3 ± 0.4 (stat.) ± 0.5 (syst.) GeV by the CMS collaboration [3].

We now begin our discussion on the numerical analyses by defining some Benchmark Points (BPs). In Fig.1(a), we display the variation of the lightest Higgs boson mass (M_{h_1}) as a function of the phase ϕ_3 , while keeping $\phi_{A_f} = \pi/2$ ($f = t, b, \tau$). The upper two curves represent two

characteristic BPs (BP-1 & BP-2, see Tab.2) obtained from the scan of the CPV-MSSM parameter space represented by eq.(11), whereas the lower two curves represent the CPX scenario [66,97,114,115]. In Fig.1(b), we present a similar variation of the lightest Higgs boson mass M_{h_1} with the CPV phase but this time with different combinations of phases for the BP-2 as displayed in Tab.2. From Fig.1, it is clear that the mass of the Higgs boson crucially depends on the CPV phases. In particular, notice that the radiative corrections to the lightest Higgs boson h_1 mass strongly depend on the stop mixing parameter $X_t = A_t - \mu \cot \beta$. Now, in our case, μ is real while A_t is a complex quantity. Hence, for different choice of phases, X_t can change, resulting in significant variations of the Higgs mass as illustrated by the red (dash-dotted) and blue (small-dash) curves.

BP	M_1	M_2	M_3	$\tan \beta$	M_{H^\pm}	M_{Q3}	M_{D3}	M_{L3}	A_t	μ	M_{h_1}
1	496.7	356.1	1200	7.7	268.6	758.2	889.3	125.6	2458.0	796.6	125.5
2	469.7	456.8	1200	9.4	294.2	1371.8	704.5	1221.6	2621.7	1179.2	125.9

Table 2: Two BPs obtained after performing a random scan over the CPV-MSSM parameter space using CPsuperH. In addition to the parameters relevant to describe the Higgs sector, we have also presented the mass of the lightest neutral Higgs boson h_1 . We have fixed the CPV phases to 90° . All masses, A_t and μ are expressed in units of GeV.

In Tab.2, we have listed the details of BP-1 and BP-2, where the last column gives the mass of the lightest neutral Higgs boson. These two points are illustrative of the fact that it is always possible to have the lightest Higgs boson mass around 125 GeV when one includes the sizeable corrections coming from the CPV phases onto the MSSM results.

Before proceeding to analyze some LHC observables, it is important to take a look at the CPV-MSSM parameters and the particle spectrum after constraints are enforced upon the points obtained in the random scan with eq.(11). In Fig.2(a) and (b) we have shown the allowed region in the $\tan \beta - M_{H^\pm}$ and $M_{h_1} - M_{h_2}$ planes, respectively. The brick red/grey points are allowed by the set of constraints mentioned in eq.(5) to eq.(8) while the black dots represent points which in addition to those constraints also satisfy the EDM constraint given in eq.(9). We find that once we impose the d_e constraint as given in eq.(9), the allowed parameter space shrinks to the region depicted by the black dots, still with sufficient regions in the parameter space surviving all the constraints. From Fig.2(a) one can conclude that the current limit on $Br(B_s \rightarrow \mu^+ \mu^-)$ prefers low to medium values of $\tan \beta \sim 6 - 13$ and a somewhat heavy charged Higgs mass $M_{H^\pm} \gtrsim 200$ GeV (brick red/grey points). In the CPC-MSSM, one has $Br(B_s \rightarrow \mu^+ \mu^-) \propto \tan \beta^6 / M_A^4$, where M_A is the pseudoscalar Higgs boson mass. Hence, to satisfy the current limit on $Br(B_s \rightarrow \mu^+ \mu^-)$, one requires a heavier M_{H^\pm} and a lower $\tan \beta$. One may expect modifications in this formula in the presence of CPV phases, however phases will not change it significantly. Fig.2(b) shows that, when the lightest Higgs boson is SM-like, the second lightest Higgs boson can have mass around 200–300 GeV. This mass window may be accessible at the 14 TeV LHC run via $gg \rightarrow h_2 \rightarrow h_1 Z$, followed by $h_1 \rightarrow b\bar{b}$ and $Z \rightarrow \nu\bar{\nu}$ or $\ell^+ \ell^-$, as the analysis is very similar to the one performed in the case

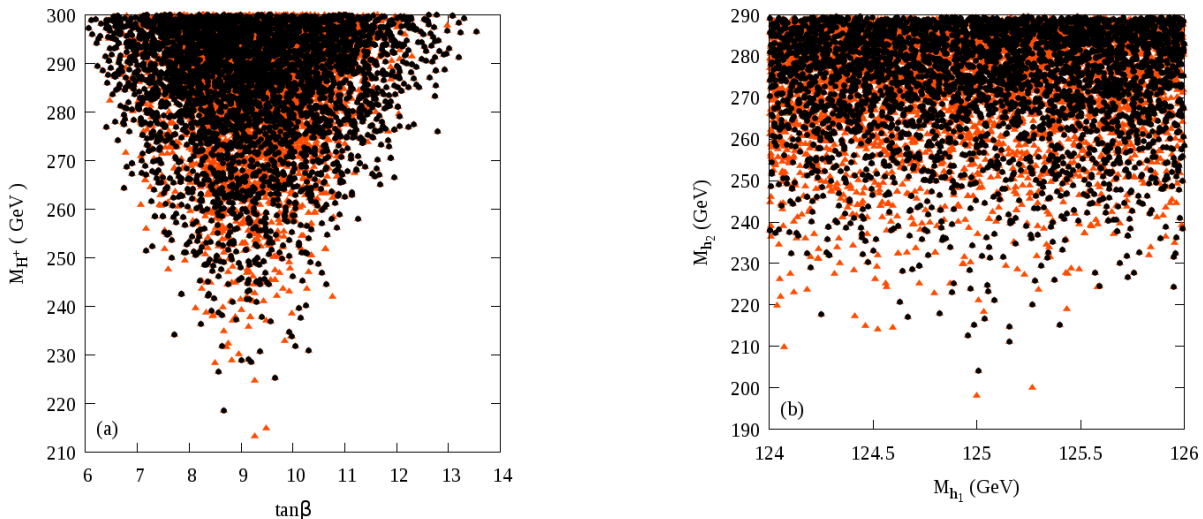


Figure 2: Constraints on the (a) $\tan\beta - M_{H^\pm}$ plane and (b) $M_{h_1} - M_{h_2}$ plane obtained after scanning the CPV-MSSM parameter space randomly. The brick red/grey triangles are allowed by the set of constraints mentioned in eq.(5) to eq.(8) while black points represent points which in addition to those constraints also satisfy the EDM constraint given in eq.(9).

of the heavy Higgs boson searches at the LHC in the CPC-MSSM [21].

We further proceed to check how the most updated d_e measurements affect the scanned CPV-MSSM parameter space. We find that, the latest bound on the d_e , quoted in eq.(10), completely negates the parameter space region corresponding to eq.(11). However, we shall see that relaxing the CPV phases from their maximal values (90°), and with more appropriate choices of the parameters, one can satisfy the latest d_e bound along with all other EDM constraints (mentioned in Tab.1) and the low energy experimental bounds. Without moving further with the results corresponding to this set of parameters (eq.(11)), we now proceed for a new scan with modified parameter set, in order to satisfy all the constraints discussed before including the stronger electron EDM bound.

4.2 Scan 2: allowing CPV phases to vary in the range of $0^\circ - 90^\circ$

Moving away from the maximal CPV scenario (where ϕ_3 and ϕ_{A_f} are fixed to 90°), sample test scans varying the magnitude of M_3 and the CPV phases (ϕ_3 , ϕ_{A_t} , ϕ_{A_b} and ϕ_{A_τ}) between $0^\circ - 90^\circ$, were performed to optimize the parameter ranges suitable to accommodate all the experimental constraints coming from the flavor sector and the EDM measurements. After a dedicated analysis using those sample data sets, we fix the ranges (upper and lower limits) of the CPV parameters and then proceed to scan the CPV parameter space for larger statistics. In our second scan, we

choose an extended M_{H^\pm} mass range by setting the upper extreme to 1000 GeV, which was fixed at 300 GeV in our first scan, in order to avoid the loss of significant amount of parameter space due to the 300 GeV upper bound on M_{H^\pm} . Similarly for $\tan\beta$ we now choose the range to be from 1 to 30, as our first scan has already discarded regions with very large values of $\tan\beta$.

We consider the following set of parameters in our final scan and vary them randomly within the specified ranges:

$$\begin{aligned}
1 < \tan\beta < 30, & & 250 \text{ GeV} < M_{H^\pm} < 1000 \text{ GeV}, \\
50 \text{ GeV} < |M_1| < 500 \text{ GeV}, & & 100 \text{ GeV} < |M_2| < 1000 \text{ GeV}, \\
800 \text{ GeV} < |M_3| < 2000 \text{ GeV}, & & 500 \text{ GeV} < |\mu| < 1000 \text{ GeV}, \\
1500 \text{ GeV} < A_t < 3000 \text{ GeV}, & & 500 \text{ GeV} < A_b, A_\tau < 3000 \text{ GeV}, \\
500 \text{ GeV} < M_{Q3} < 1500 \text{ GeV}, & & 1000 \text{ GeV} < M_{U3} < 3000 \text{ GeV}, \\
500 \text{ GeV} < M_{D3} < 2000 \text{ GeV}, & & 100 \text{ GeV} < M_{L3}, M_{E3} < 2000 \text{ GeV}, \\
0^\circ < \phi_3, \phi_{A_t}, \phi_{A_b}, \phi_{A_\tau} < 90^\circ. & &
\end{aligned} \tag{12}$$

We take the 800 GeV lower limit on M_3 to satisfy the experimental lower bound on the gluino mass [116]. We would like to remind our reader that the lower bound on the gluino mass is applicable for the CPC-MSSM and will change in the CPV-MSSM due to the significant modifications in different decay/Br's. However, from the current LHC results, we expect that the gluino mass bound would be in the TeV regime and so, to be in a conservative side, we choose 800 GeV as the lower limit. The ranges for μ , A_t , M_{Q3} and M_{U3} are set consulting sample test scans which favor relatively large values of A_t and small values of the Higgsino mass parameter μ . We allow the CPV phases ($\phi_3, \phi_{A_t}, \phi_{A_b}, \phi_{A_\tau}$) to vary between 0° to 90° independently and randomly. Other remaining parameters in this second scan are identical to those of the previous one (Scan 1).

With these new set of CPV-MSSM parameter ranges, we scan the parameter space for around 10^7 points and impose all the experimental constraints starting from eq.(5) to eq.(8) and the latest bounds on d_e (eq.(10)), d_{Tl} , d_n and d_{Hg} (Tab.1), after the primary selection criterion on the Higgs boson mass. In Fig.3(a) and 3(b), we present the allowed region in the $\tan\beta - M_{H^\pm}$ and $M_{h_1} - M_{h_2}$ planes, respectively, for the parameter ranges mentioned in eq.(12). Clearly, larger M_{H^\pm} values can accommodate larger $\tan\beta$, possibly even going beyond 30, satisfying all the constraints. From Fig.3(a) we can see that values of $\tan\beta$ smaller than around 5 are not allowed. In order to understand which constraint disallows $\tan\beta$ below 5, we plot the points allowed by the different set of constraints, where magenta/medium grey dots are the points without any experimental bound, the cyan/light grey dots are the points which obey only the Higgs mass bound and the black points are allowed by all the experimental constraints starting from eq.(5) to eq.(8) and the latest bounds on d_e (eq.(10)), d_{Tl} , d_n and d_{Hg} (Tab.1). It is clear that the Higgs mass bound itself puts a lower limit of $\tan\beta \sim 5$. Here we would like to mention that, this pattern is consistent with the CPC-

MSSM, see Ref. [142]. Fig.3(b) says that the second lightest Higgs boson (h_2) can be as heavy as the H^\pm , with a preference for heavier masses.

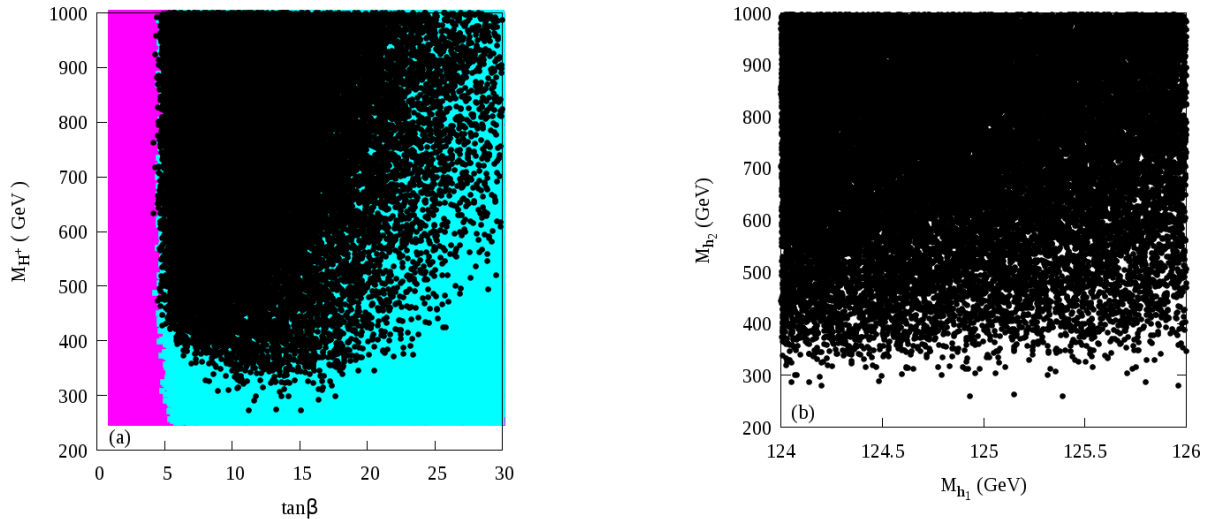


Figure 3: Constraints on the (a) $\tan\beta - M_{H^\pm}$ and (b) $M_{h_1} - M_{h_2}$ plane respectively, obtained after scanning the CPV-MSSM parameter space randomly, for the input parameters mentioned in eq.(12). The magenta/medium grey region is without any experimental constraint, the cyan/light grey region is allowed only by the primary Higgs mass bound and the black points are allowed by the set of constraints mentioned in eq.(5) to eq.(8) and also the d_e (eq.(10)), d_{TI} , d_n and d_{Hg} (Tab.1) constraints.

In Fig.4 we plot the allowed points in the (a) $\phi_{A_t} - \phi_3$ and (b) $\phi_{A_t} - \phi_{A_b}$ planes. We get that most of the allowed points fall in the region with relatively smaller values of ϕ_{A_t} and ϕ_3 , even though there are some points with large phase values as well. Here we would like to note that there were no surviving points in the first scan (corresponding to eq.(11)) with $\Phi_{A_t} = \Phi_{A_b} = \Phi_{A_\tau} = \phi_3$ fixed at 90° . In the present scan the large M_{H^\pm} values make it possible to evade the experimental constraints for large values of the CPV phases. Fig.4(b) clearly shows that ϕ_{A_b} has negligible effect. A similar result is obtained also for ϕ_{A_τ} , which is not presented here.

Fig.5(a) and (b) summarize the spectrum of some relevant particles in the context of the CPV-MSSM under the same conditions as previously explained, with the same black color code as in Fig.3. Fig.5(a) shows, in particular, that the lightest chargino and neutralino masses could be as high as 900 GeV and 500 GeV respectively, while Fig.5(b) says that the lightest stop and stau masses could be as low as 450 GeV and 100 GeV respectively satisfying all the present experimental bounds.

To study the constraints coming from the flavor sector, in Fig.6(a) we show the dependence of $Br(b \rightarrow s\gamma)$ on the charged Higgs boson mass, with and without the imposition of the EDM

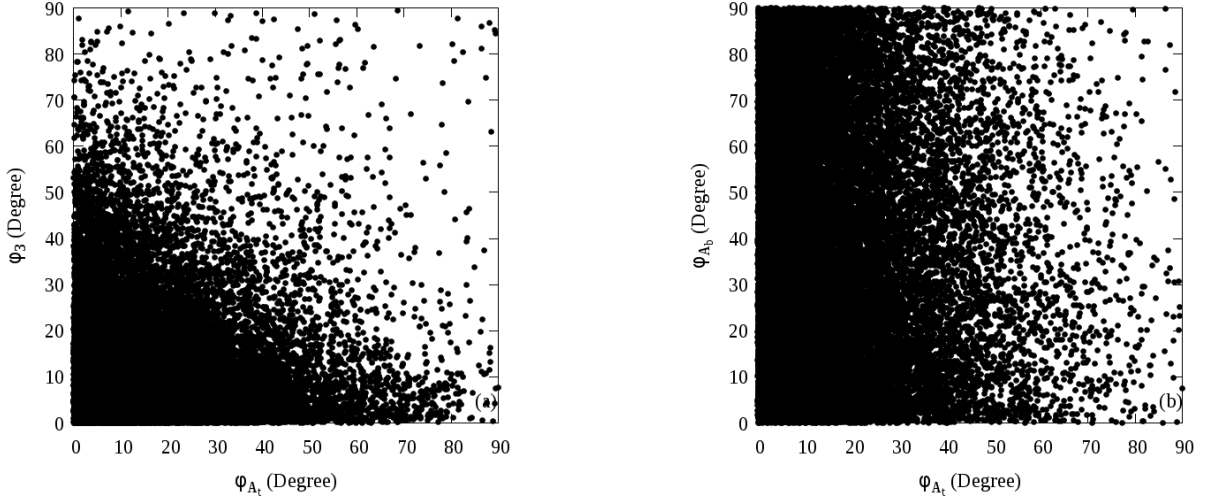


Figure 4: Correlation of ϕ_{A_t} with (a) ϕ_3 and (b) ϕ_{A_b} . The black color code is same as in Fig.3.

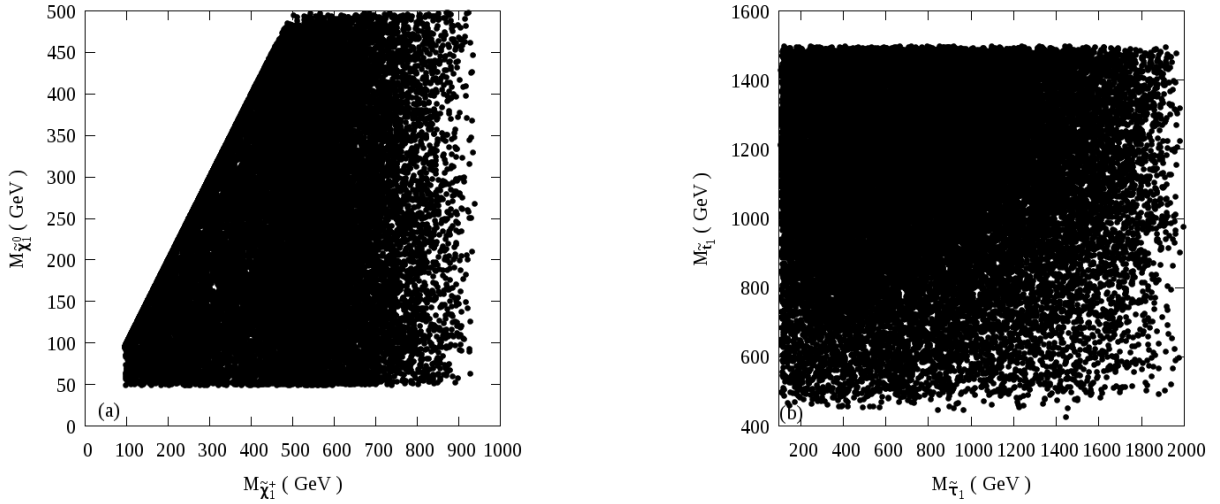


Figure 5: (a) $M_{\tilde{\chi}_1^\pm} - M_{\tilde{\chi}_1^0}$ and (b) $M_{\tilde{\tau}_1} - M_{\tilde{t}_1}$ planes after imposing all our selection criteria. The black color code is same as in Fig. 3.

constraints. Similar kind of correlation can be seen in Fig.6(b), where we plot the variation of $Br(B_s \rightarrow \mu^+ \mu^-)$ with $\tan \beta$. The black color code is the usual one which represents the points satisfying all the constraints, while the brick red/grey points satisfy all the experimental bounds starting from eq.(5) to eq.(8), except the EDM constraints, mentioned in eq.(10) and Tab.1. We have already discussed in Sec.3 that significant amount of SUSY contribution may come from the charged Higgs loop and the chargino loop in $b \rightarrow s\gamma$ decay, and cancellation between the SUSY

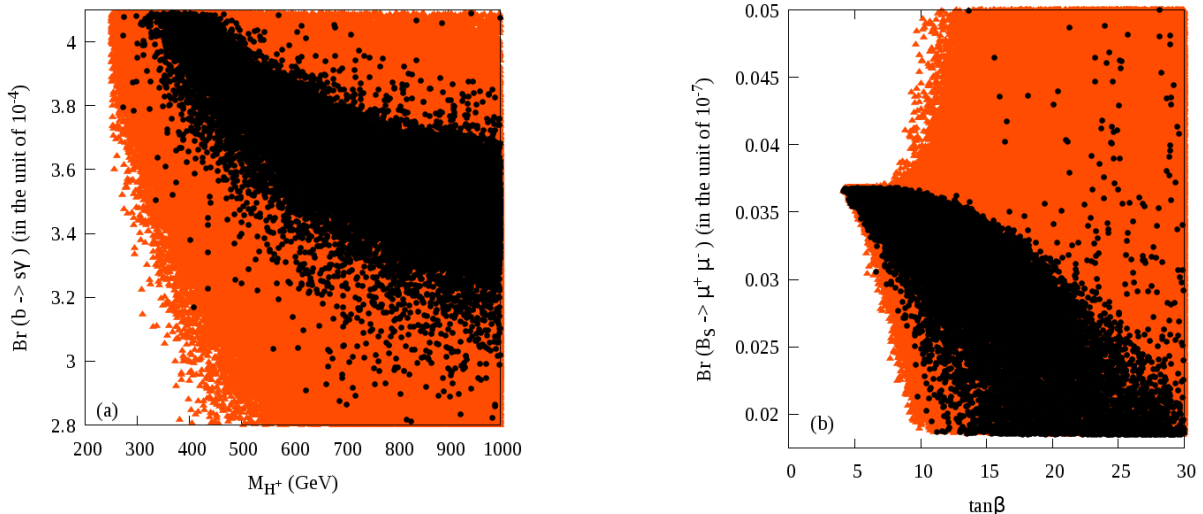


Figure 6: Variation of $Br(b \rightarrow s\gamma)$ with the charged Higgs mass (a) and the correlation between $Br(B_s \rightarrow \mu^+\mu^-)$ and $\tan\beta$ (b). The black colored points satisfy all the constraints, while the brick red/grey points correspond to the points satisfying all of the constraints except the EDM ones.

contribution and the SM value may occur, resulting in enhancement/suppression in the decay width. On the other hand, the SUSY contribution to the flavor changing $b \rightarrow s$ couplings, present in the $Br(B_s \rightarrow \mu^+\mu^-)$ decay, strongly depends on $\tan\beta$. From both Fig.6(a) and Fig.6(b), we find that the recent electron EDM measurements affect the CPV parameter space significantly, specially the region with large $\tan\beta$. The generic SUSY contribution to the electron EDM comes from charginos, neutralinos at the one loop level and from neutral Higgses at the two loop level. One can significantly reduce the one loop contributions by making the first two generations of sfermions very heavy (around 5 - 10 TeV). However, the Higgsino contribution is always present and it strongly depends on the Higgs boson coupling with the down type fermions and the coupling grows with $\tan\beta$. So, we find that the imposition of the current d_e bound strongly discards the large $\tan\beta$ regime and thereby affect both the rare b-decays $b \rightarrow s\gamma$ and $B_s \rightarrow \mu^+\mu^-$ significantly. Apart from the $\tan\beta$ effect, non-trivial effects coming from the different loops associated with the different SUSY particles also play crucial role in accepting/discarding the parameter space points.

In Fig.7(a), we show the correlation in the $\Delta M_{B_d}^{\text{SUSY}} - \Delta M_{B_s}^{\text{SUSY}}$ plane where these quantities measure the SUSY contributions to the $B_d^0 - \bar{B}_d^0$ and $B_s^0 - \bar{B}_s^0$ mass differences, respectively. From the figure, it is clear that all the points, which survive the Higgs mass cut and the low energy flavor data, are well within the experimental 3σ limit. This figure also justifies our choice of neglecting the $\Delta M_{B_s}^{\text{SUSY}}$ cut as a selection criterion. However, with reduced theoretical uncertainty, this constraint will play a significant role in the CPV-MSSM parameter space. Finally, in Fig.7(b) we show the variation of the electron EDM with the phase of A_t , namely ϕ_{A_t} . We find that the current experimental electron EDM limit mostly favors smaller values of the CPV phases, though

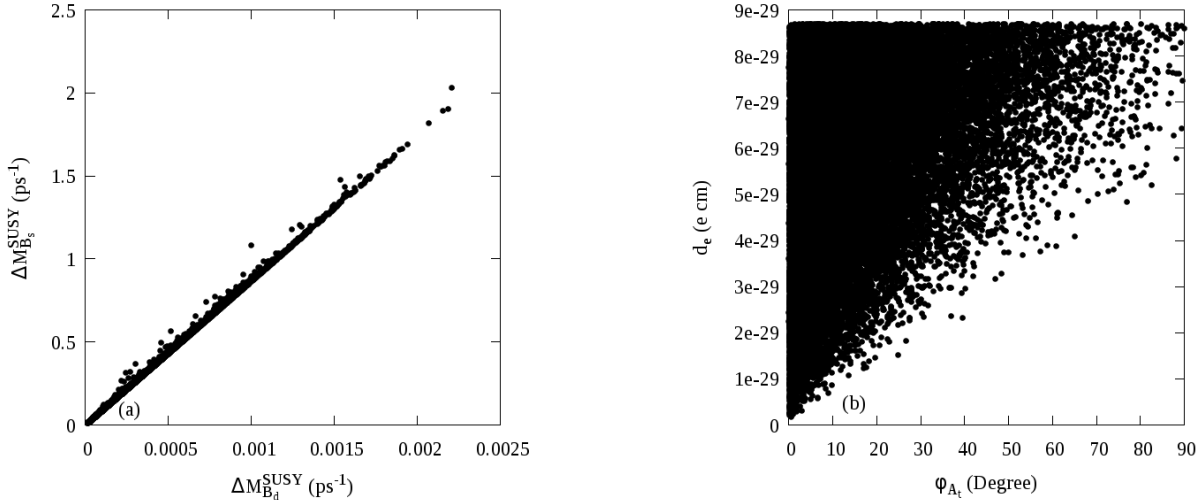


Figure 7: The left panel displays the correlation in the $\Delta M_{B_d}^{\text{SUSY}} - \Delta M_{B_s}^{\text{SUSY}}$ plane, while the right panel shows the impact of the CPV phase ϕ_{A_t} on the electron EDM. The color code is same as in Fig.3.

few parameter points may signal large phase values. We also find similar kind of behavior for all other EDMs against the relevant CPV phases.

5 Results for the LHC Higgs signals

We shall now present the compatibility of the selected parameter space regions with the LHC measurements specific to the discovered Higgs boson resonance. As the first scan is found to be incompatible with the EDM bounds, we shall focus our attention on the second scan. The results presented in this section are, therefore, those from the second scan, unless explicitly mentioned.

At the LHC, the Higgs boson is dominantly produced via Gluon-Gluon Fusion (GGF), which at the lowest order occurs at one-loop level, with the Higgs boson subsequently decaying into $\gamma\gamma$ or $ZZ^* \rightarrow 4\ell$ or $WW^* \rightarrow \ell\nu\ell\nu$ ⁵. Now, the leading contribution of Higgs boson decays into ZZ^* is via a tree-level process, whereas the Higgs decays into the di-photon final state via a one-loop process at leading order. This one-loop decay process potentially contains SUSY particles like stop, sbottom, stau, charginos and charged Higgs bosons in addition to the SM particles (top, bottom and charged gauge bosons). Conversely, in the GGF production mode only colored particles (top, bottom, stop and sbottom) contribute to the loop. Assuming the Narrow Width Approximation

⁵We neglect here the consideration of the $\tau^+\tau^-$ and $b\bar{b}$ decay modes from GGF, as corresponding experimental errors are still very large.

(NWA)⁶ and neglecting higher order QCD corrections at production level⁷, we define the Higgs boson event ratios as follows:

$$R_{XX} = \frac{\Gamma(h_1 \rightarrow gg)^{\text{CPV-MSSM}}}{\Gamma(h \rightarrow gg)^{\text{SM}}} \times \frac{\text{Br}(h_1 \rightarrow XX)^{\text{CPV-MSSM}}}{\text{Br}(h \rightarrow XX)^{\text{SM}}}, \quad (13)$$

where, $XX = \gamma\gamma$ or ZZ^* or WW^* and h_1 is the lightest Higgs boson of the CPV-MSSM, while in the SM case it is marked as h .

Turning our attention to the study of effects specifically due to the CPV phases, notice that CPV effects enter into eq.(13) through higher order corrections in the definition of the physical h_1 mass as well as through lowest order terms via the $h_1 \tilde{f} \tilde{f}^*$ couplings, where \tilde{f} refers to any possible sfermion. In fact, as emphasized in Refs. [46–52], the most significant CPV effects are induced by the latter, since the former is responsible for mass shifts between models which are within current experimental uncertainties in the determination of the resonant Higgs mass.

In order to appreciate such specific CPV effects in our analysis, we find it convenient to study the ratio of the bottom/top Yukawa coupling for the h_1 state of the CPV-MSSM relative to SM values for the h_1 boson, which can be written as ($q = b, t$):

$$\frac{y_q^{\text{CPV-MSSM}}}{y_q^{\text{SM}}} = R_{q-S} + i\gamma_5 R_{q-PS}. \quad (14)$$

Here R_{q-S} and R_{q-PS} denote the scalar and pseudoscalar part of the Higgs Yukawa coupling, respectively. The full expressions for these terms can be found in the CPSuperH manual [139]. When $R_{\gamma\gamma}$ is plotted as a function of the b -quark couplings, R_{b-S} and R_{b-PS} , as shown in Fig.8(a) and (b), one finds that there are solutions to the LHC Higgs data with both positive and negative values of R_{b-S} , which is typical of the CPV-MSSM, unlike the case of the CPC-MSSM, which only allows for positive values. A similar behavior is obtained for the dependence on the t -quark couplings, as shown in Fig.8(c) and (d). Further, if one recalls that the coupling of the top quark to the h_1 Higgs boson is inversely proportional to $\sin\beta$ (relative to the SM case) and that we have varied $\tan\beta$ from 1 to 30 (which implies $\sin\beta \sim 1$), it is not surprising to see that R_{t-S} remains around unity. Needless to say, by definition, R_{b-PS} and R_{t-PS} are zero in the CPC-MSSM, whereas both of them are non-zero in the CPV-MSSM, although their absolute values are much smaller than those for R_{b-S} and R_{t-S} , respectively.

We now proceed to study correlations among the different signal strength variables as mentioned above. At first, we would like to discuss the correlation of the signal strength variables corresponding to our first scan (Scan 1), although the updated results from the ACME EDM collaboration on the electron EDM excluded all the parameter space points, for the sake of completeness of the

⁶Which is justified by the fact that in all models considered (SM, CPC-MSSM and CPV-MSSM) one has that the Higgs width is always several orders of magnitude smaller than the Higgs mass.

⁷Which would induce a different finite term inside the K -factor in the SM with respect to the CPC-MSSM (and CPV-MSSM as well), though with differences generally too small to be of relevance here.

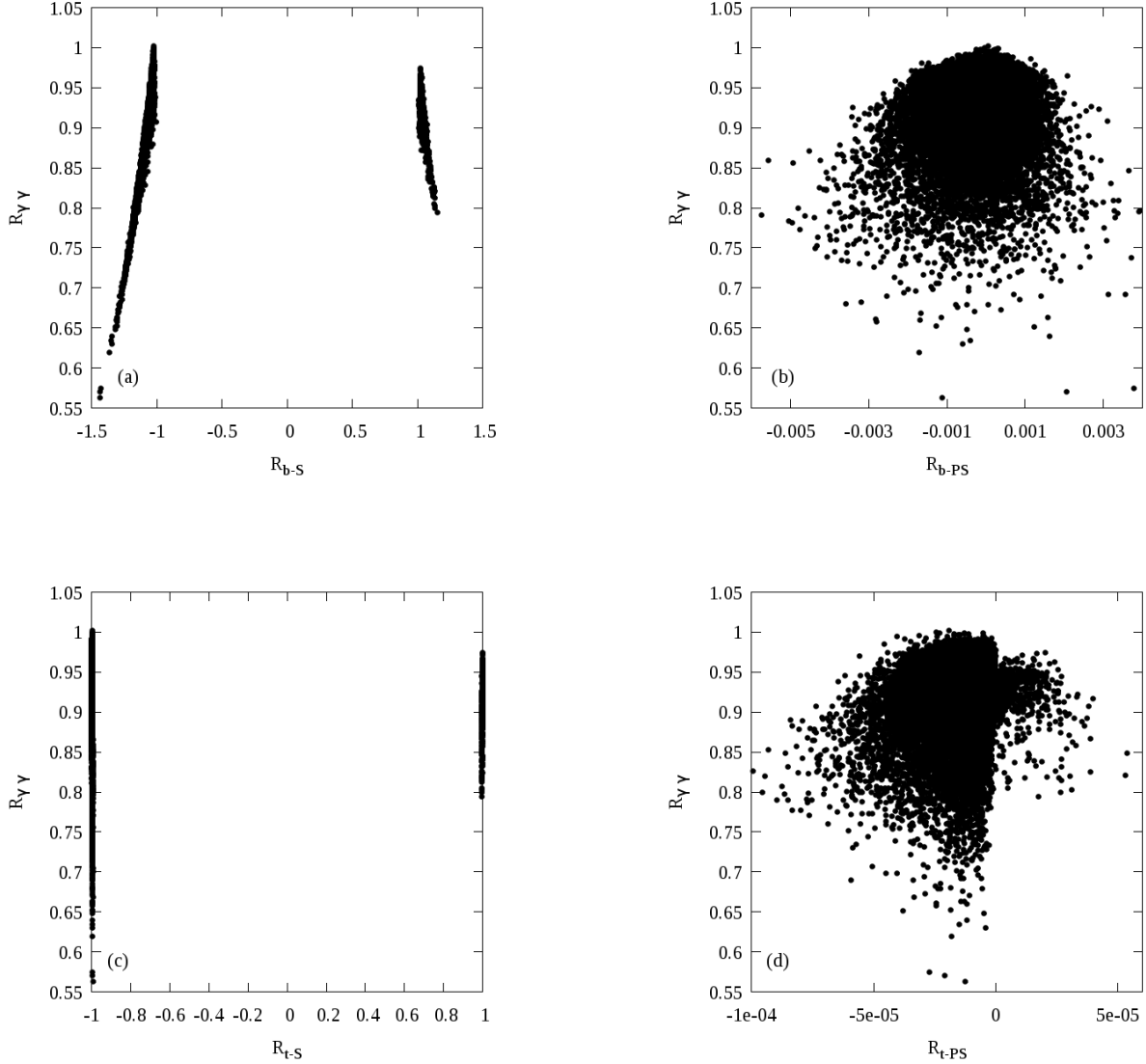


Figure 8: Variation of $R_{\gamma\gamma}$ with the scalar and pseudoscalar part of the ratio of the bottom ((a) & (b)) and top ((c) & (d)) quark Yukawa couplings defined in eq.(14) in the CPV-MSSM. The black color code is same as in Fig.3.

discussion. In Fig.9(a), we plot the correlation between R_{ZZ} and $R_{\gamma\gamma}$. Similar correlation in R_{bb} - $R_{\tau\tau}$ plane can be seen in Fig.9(b), when the Higgs boson is produced in association with a vector boson (W/Z). We then compare our results with the recent CMS data [5–7, 10]. According to the CMS collaboration, the signal strength (our event ratios) for the $\gamma\gamma$ channel is $(0.78^{+0.28}_{-0.26})$, while for the ZZ^* and WW^* channels are $(0.9^{+0.30}_{-0.24})$ and (0.68 ± 0.20) respectively [5–7, 10]. We plot our results against the corresponding CMS results using 1σ (green/medium grey patch) and 2σ (yellow/light grey patch) error bands around the experimental best-fit values (plus marks). We

find that the maximum value of $R_{\gamma\gamma}$ is ~ 0.7 while R_{bb} and $R_{\tau\tau}$ are always greater than 1. As our first scan is not compatible with the recent electron EDM bound, hence from now onwards, we again turn our attention to the results corresponding to our second scan.

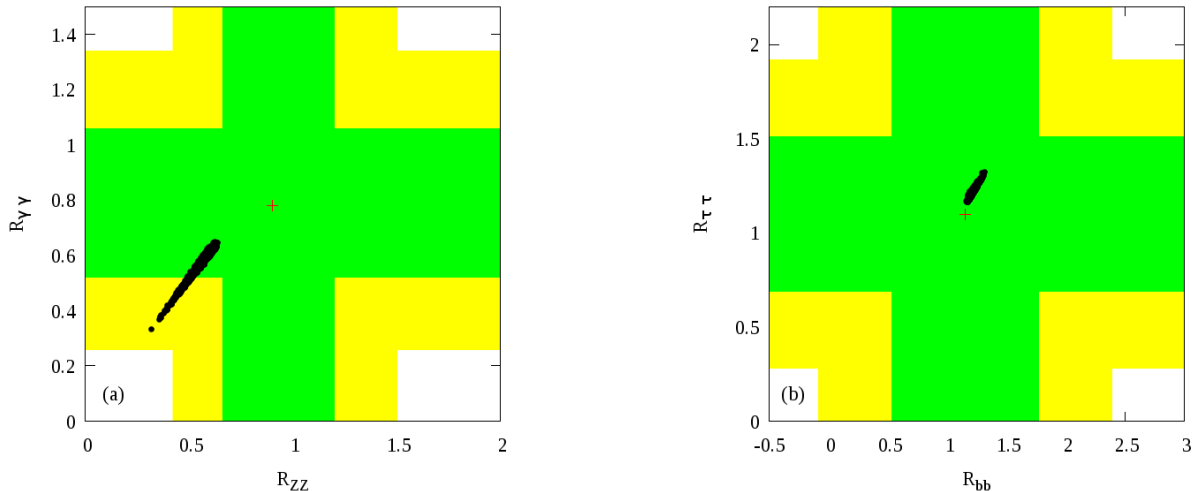


Figure 9: Correlation between (a) R_{ZZ} and $R_{\gamma\gamma}$ when the Higgs boson is produced via Gluon-Gluon Fusion (GGF) and (b) R_{bb} and $R_{\tau\tau}$ when the Higgs boson is produced via Vector Boson Fusion (VBF), presented in comparison with the recent LHC data (CMS) along with the 1σ (green/medium grey patch) and 2σ (yellow/light grey patch) error bands around the experimental best-fit values (plus marks). The black color code is same as in Fig.2. Note that this scan corresponds to a setup in which the CPV phases are maximal i.e. 90° .

We first study the correlation of $R_{\gamma\gamma}$ with R_{ZZ} and R_{WW} when the Higgs is produced via GGF channel. It is evident from Fig.10 that these values are in good agreement (within 1σ) with the latest Higgs data as obtained by the CMS collaboration [5, 6, 10] for the $h_1 \rightarrow \gamma\gamma$, $h_1 \rightarrow ZZ^*$ and $h_1 \rightarrow WW^*$ channels. The observation of the $h_1 \rightarrow b\bar{b}$ and $h_1 \rightarrow \tau^+\tau^-$ decays using GGF production mode are considered nearly impossible due to overshadow of QCD di-jet events. Hence, to discuss signal strength variables associated with the bottoms and taus, we assume the Higgs production in association with a vector boson (W/Z) and the gauge bosons decaying leptonically with the Higgs boson decaying to a pair of b -jets, as both CMS and ATLAS have some sensitivity in this channel [8, 9, 14, 15]. In this case, the definition of the corresponding event ratios will be modified to (here, $V = W/Z$):

$$R_{YY} = \frac{\Gamma(h_1 \rightarrow VV)^{\text{CPV-MSSM}} \text{Br}(h_1 \rightarrow YY)^{\text{CPV-MSSM}}}{\Gamma(h \rightarrow VV)^{\text{SM}} \text{Br}(h \rightarrow YY)^{\text{SM}}}, \quad (15)$$

where $YY = b\bar{b}$, $\tau^+\tau^-$.

The CMS collaboration results on these decay channels are $R_{bb} = 1.15 \pm 0.62$ and $R_{\tau\tau} = 1.10 \pm 0.41$ [10], respectively. In Fig.11 we display the scatter plots in the (a) the $R_{bb} - R_{\gamma\gamma}$ plane

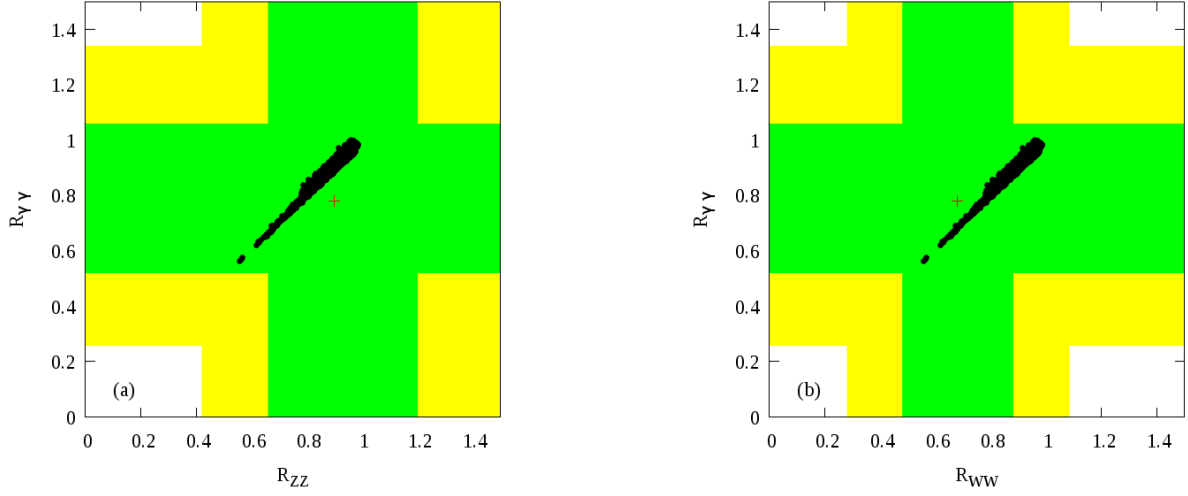


Figure 10: Correlation of $R_{\gamma\gamma}$ with (a) R_{ZZ} and (b) R_{WW} , when the Higgs boson is produced via GGF, in comparison to the latest LHC data (CMS) along with the error bands (the yellow/light grey and green/medium grey patches are the 2σ and 1σ uncertainty levels, respectively, around the experimental best-fit values, represented by the plus marks). The black color scheme is same as in Fig.3.

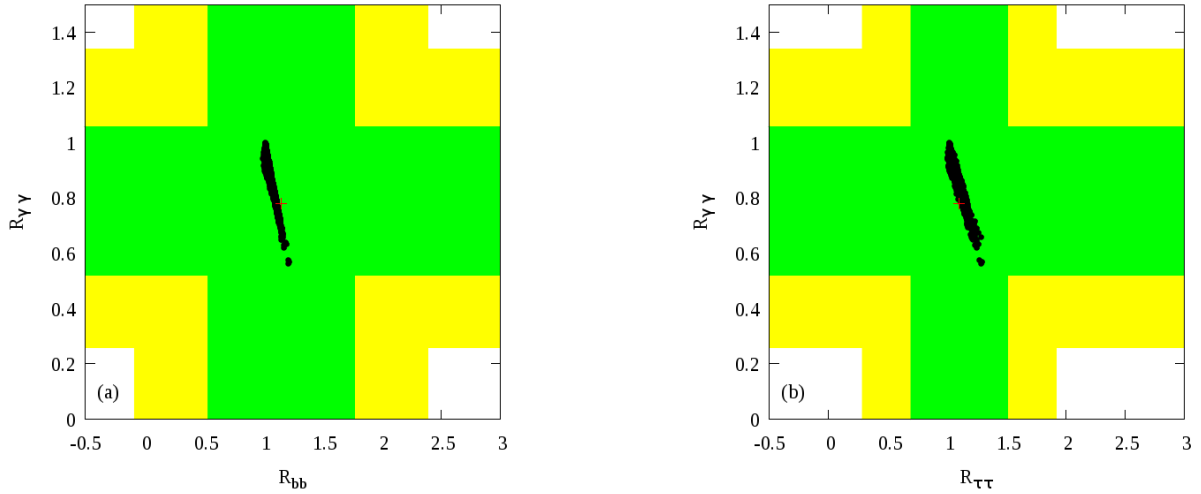


Figure 11: (a) R_{bb} vs $R_{\gamma\gamma}$ and (b) $R_{\tau\tau}$ vs $R_{\gamma\gamma}$ with the best-fit corresponding CMS values (plus marks). The yellow/light grey and green/medium grey patches are the 2σ and 1σ uncertainty bands, respectively. The black color scheme is same as in Fig.3.

and (b) $R_{\tau\tau} - R_{\gamma\gamma}$ plane, with the CMS results. The color scheme is same as earlier. We note that the QCD and SUSY QCD corrections to M_b (Δ_b) play important roles in modifying the total decay

width as well as the relevant Br 's of the Higgs boson [23, 143, 144]. This primarily changes the $h_1 \rightarrow b\bar{b}$ coupling values which are reduced for large Δ_b ⁸. In general, a reduction (enhancement) of the $h_1 \rightarrow b\bar{b}$ coupling decreases (increases) the total decay width of the Higgs boson. This in turn enhances (reduces) the Br 's to modes like $h_1 \rightarrow \gamma\gamma$ thereby increasing (decreasing) $R_{\gamma\gamma}$ [23]. This is evident in Fig.11(a) that shows an anti-correlation between the values of $R_{\gamma\gamma}$ and $R_{b\bar{b}}$. A similar kind of anti-correlation exists in Fig.11(b) where we show the variation in the $R_{\tau\tau} - R_{\gamma\gamma}$ plane. The plus marks represent the experimental best-fit values (CMS) for $R_{b\bar{b}}$ and $R_{\tau\tau}$ [10], with 1σ and 2σ error levels (green/medium grey and yellow/light grey patches, respectively).

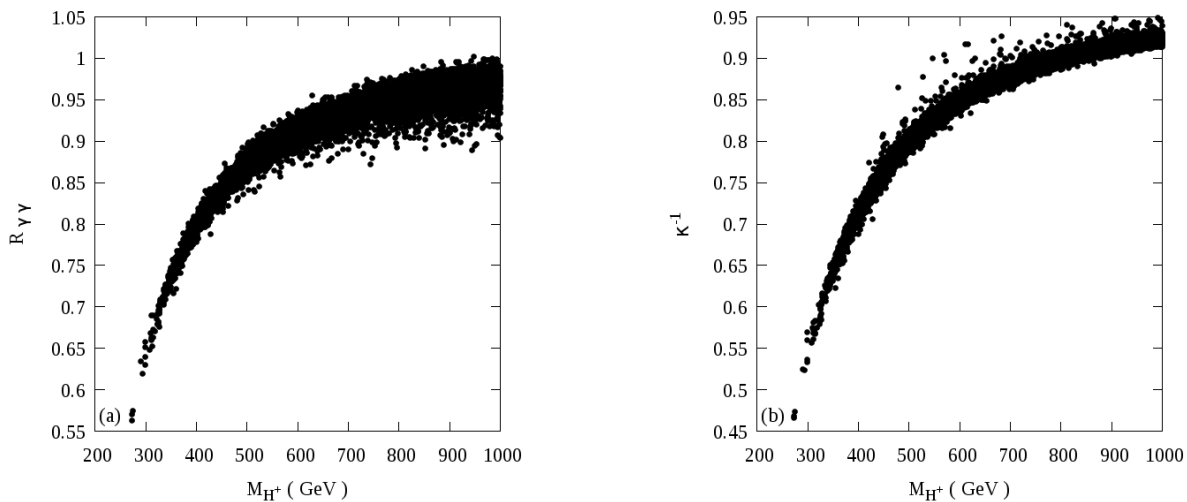


Figure 12: The correlations between (a) M_{H^\pm} and $R_{\gamma\gamma}$, (b) M_{H^\pm} and κ_{bb}^{-1} . We define κ_{bb} as $\kappa_{bb} \equiv \Gamma(h \rightarrow b\bar{b})/\Gamma(h \rightarrow b\bar{b})^{\text{SM}}$. The black color scheme is same as in Fig.3.

As in our second scan (Scan 2) we increase M_{H^\pm} to 1 TeV, we find it interesting to investigate the role of the charged Higgs mass in the Higgs to di-photon decay. The charged Higgs boson contribution to the di-photon amplitude is usually negligible compared to the fermion and gauge boson loop contributions [40]. In Fig.12(a) we show the variation of $R_{\gamma\gamma}$ with M_{H^\pm} and find that the charged Higgs contribution increases the $R_{\gamma\gamma}$ value. However, we find that the key role of the H^\pm mass in $R_{\gamma\gamma}$ does not come from the $h\gamma\gamma$ coupling, rather it comes from the modification in the total decay width of the Higgs and the $hb\bar{b}$ coupling. To understand this behavior, we define a quantity κ_{bb} as $\kappa_{bb} \equiv \Gamma(h \rightarrow b\bar{b})/\Gamma(h \rightarrow b\bar{b})^{\text{SM}}$ keeping in mind that $\Gamma_{\text{tot}} \approx \Gamma(h \rightarrow b\bar{b})$. In Fig.12(b), we plot κ_{bb}^{-1} with M_{H^\pm} and find a strong correlation between them. We observe that κ_{bb} is large for smaller values of M_{H^\pm} and it decreases with the increase of M_{H^\pm} . Since κ_{bb} is proportional to $\Gamma(h \rightarrow b\bar{b}) \approx \Gamma_{\text{tot}}$, hence decrease in κ_{bb} implies decrease in total decay width, which in turn implies

⁸Notice that Δ_b is typically positive for this analysis with positive μ [144].

enhancement in Higgs to di-photon branching ratio. At the tree level, the charged and pseudoscalar Higgs boson masses are related as $m_{H^\pm}^2 = m_A^2 + m_{W^\pm}^2$. In the CPC-MSSM, the $hb\bar{b}$ coupling, at tree level, goes as $\sin \alpha / \cos \beta$, where α and β angles are related as:

$$\tan 2\alpha = \tan 2\beta \frac{m_{H^\pm}^2 - m_{W^\pm}^2 + m_Z^2}{m_{H^\pm}^2 - m_{W^\pm}^2 - m_Z^2}. \quad (16)$$

From the above relation, it is obvious that the mixing angle α is also dependent on M_{H^\pm} and any change in this parameter can lead to a change in κ_{bb} , which in turn modify the $\Gamma(h \rightarrow b\bar{b})$ and also Γ_{tot} .

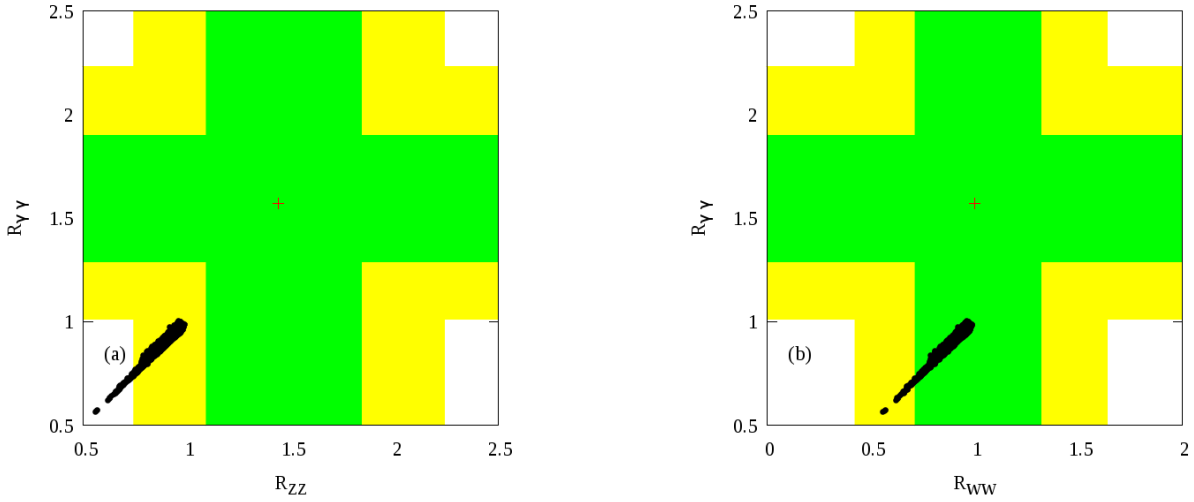


Figure 13: Results on $R_{\gamma\gamma}$, R_{ZZ} and R_{WW} , presented with the corresponding ATLAS results in (a) $R_{ZZ} - R_{\gamma\gamma}$ and (b) $R_{WW} - R_{\gamma\gamma}$ planes. The plus marks are the best-fit experimental values. The green/medium grey and yellow/light grey patches are 1σ and 2σ uncertainty levels, and the color scheme is same as before.

The updated ATLAS results for the signal strengths of the aforementioned channels are: $R_{\gamma\gamma} = 1.57_{-0.28}^{+0.33}$, $R_{ZZ} = 1.44_{-0.35}^{+0.40}$, $R_{WW} = 1.00_{-0.29}^{+0.32}$, $R_{bb} = 0.2_{-0.6}^{+0.7}$ and $R_{\tau\tau} = 1.4_{-0.4}^{+0.5}$ [17]. We present and compare our results with those from ATLAS in Fig.13 and 14. From the plots it is clear that our $R_{\gamma\gamma}$ is just reaching the lower part of the 2σ region, R_{ZZ} and R_{WW} are almost within the 2σ and 1σ bands, whereas R_{bb} and $R_{\tau\tau}$ are within the 2σ and 1σ error bands respectively, about the best-fit experimental values from the ATLAS. However, note that there are indeed significant discrepancies between the CMS and ATLAS results and our results are well consistent with those from the CMS collaboration.

Before we end this section, we would like to comment on the phenomenological implications of

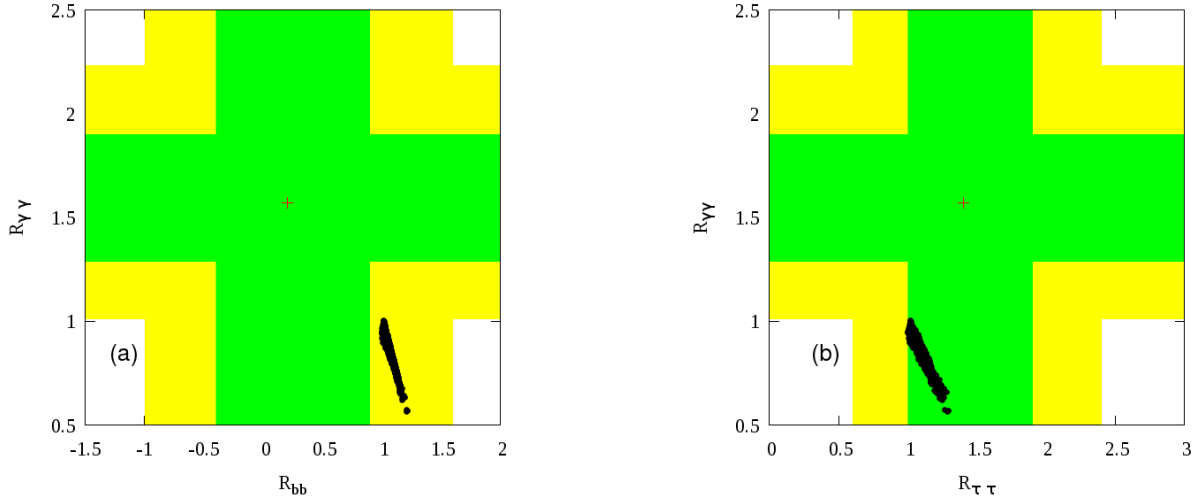


Figure 14: Results on R_{bb} and $R_{\tau\tau}$ presented with the corresponding ATLAS results in (a) $R_{bb} - R_{\gamma\gamma}$ and (b) $R_{\tau\tau} - R_{\gamma\gamma}$ plane. The green/medium grey and yellow/light grey patches are 1σ and 2σ error bands and the plus marks represent the best-fit ATLAS values for R_{bb} , $R_{\tau\tau}$ and $R_{\gamma\gamma}$.

the presence of non-zero pseudoscalar Higgs yukawa couplings. Note that, the possibility of being a pure CP-odd state for the observed Higgs particle has now been mostly ruled out [145, 146], however the option of being a mixed CP state is still an open issue [147–150]. A non-zero pseudoscalar Higgs yukawa coupling would affect several production and decay modes of the observed Higgs boson. For example, the gluon fusion process crucially depends on the Higgs couplings with the top and bottom quarks, while the decay of the Higgs to a pair of photons mostly involves the top quark coupling. A global analysis involving all the Higgs couplings and the available current LHC results have been performed with and without the current EDM constraints [149–151]. According to Ref. [149, 150], the current data cannot rule out the possibility of non-zero pseudoscalar Higgs couplings, infact it gives equally good fits compared to the CPC case. However, when current EDM bounds are considered, the Higgs pseudoscalar couplings are restricted to approximately 10^{-2} [151]. Note that, from Fig. 8(b) and (d), it is evident that our findings are in good agreement with the results obtained from a dedicated global fit. The measurement of the CP properties of the Higgs boson at the LHC mostly rely on its couplings to massive vector bosons. It has been shown in Ref. [152] that the gluon fusion process could be sensitive enough at the 14 TeV run of the LHC to study the CP properties of the Higgs boson. In fact, the presence of non-trivial CPV Higgs couplings would have important implications in the electroweak baryogenesis [153].

6 Conclusions

The discovery of a Higgs-like resonance with a mass close to 125 GeV by both the multi-purpose experimental collaborations ATLAS and CMS operating at the LHC created a great interest in understanding the ultimate means adopted by nature for mass generation. The precise determination of its spin, CP properties and couplings to the SM fermions and gauge bosons are highly crucial to know the exact dynamics of electro-weak symmetry breaking. Although the measurements done so far indicate that this Higgs-like boson is compatible with the SM hypothesis, however due to large uncertainties in some of the Higgs detection channels, one still has the possibility of testing this object as being a candidate of some BSM physics.

With this motivation in mind, we scan the CPV-MSSM parameter space in order to accommodate the 125 GeV Higgs boson with signal event rates consistent with the observed LHC data and all other available experimental bounds till date. It is well known that any new source of CP violation (above and beyond what is embedded in the SM) would lead to additional contributions to the various EDMs. Therefore, while scanning the CPV-MSSM parameter space, we also enforce different EDM constraints, namely the electron, neutron, Mercury and Thallium EDMs. In addition, we vary the CPV phases of the gaugino mass parameter M_3 , trilinear couplings A_t, A_b and A_τ from 0° to 90° . Note that we set other CPV phases like ϕ_1 (phase of M_1), ϕ_2 (phase of M_2), phases of the first two generations of fermions to zero since these variables affect the Higgs sector negligibly. We further impose several low energy constraints, mainly coming from the different heavy flavor physics processes.

We perform two separate parameter space scans: (a) with some of the CPV phases to their maximal value (90°) and (b) varying these phases from 0° to 90° . For both these two scans, other parameters vary randomly within some specified ranges. We see that maximal phase scenario (case (a)) is ruled out by the current EDM measurements, specially updated electron EDM measurement. However, we find significant amount of parameter space points, in case (b), satisfying all the constraints including EDMs. As expected, we see that relatively smaller values (c.f. Fig.7(b)) of these CPV phases are favored by the EDM constraints. We also calculate the signal rates of the Higgs boson in the $gg \rightarrow h_1 \rightarrow \gamma\gamma$, $gg \rightarrow h_1 \rightarrow ZZ^* \rightarrow 4\ell$, $gg \rightarrow h_1 \rightarrow WW^* \rightarrow \ell\nu\ell\nu$, $pp \rightarrow Vh_1 \rightarrow Vb\bar{b}$ and $pp \rightarrow Vh_1 \rightarrow V\tau^+\tau^-$ ($V \equiv W^\pm, Z$) channels and find that over a large expanse of parameter space of CPV-MSSM, our results are compatible (within 1σ) with the observed data from the CMS collaboration, while most of them are still consistent within 2σ of the ATLAS results.

Although, our results do not differ significantly from those of the CPC-MSSM, which are available in the literature. However, we find some interesting results in terms of some of the observables of CPV-MSSM. The couplings of the Higgs boson with the bottom quark and top quark are very important to claim the discovery of the observed particle as the SM Higgs boson. We find that the

imaginary part of the top and bottom Yukawa couplings can take very small but non-zero values even after satisfying all the recent updates from both the CMS and ATLAS collaborations (in terms of the signal strength variable μ , or R in our case) within $1 - 2\sigma$ uncertainty. Moreover, we also find an interesting result from the correlation plots of the different signal strength variables. We do not find any significant excess in the di-photon decay mode (in both scan 1 and scan 2), but we do see excess of events over the SM predictions for both the $b\bar{b}$ and $\tau^+\tau^-$ decay modes, i.e., in R_{bb} and $R_{\tau\tau}$, when the Higgs boson is produced in association with the SM gauge bosons W or Z . The suppression in the di-photon decay mode with simultaneous enhancement in $b\bar{b}$ and $\tau^+\tau^-$ decay modes with respect to the SM prediction and presence of non-zero imaginary parts of the top and bottom Yukawa couplings, could be an interesting signature of this model. We briefly discuss the phenomenological implications of the presence of such non-zero pseudoscalar Higgs coupling. In addition to that, we also find that it is possible to have a Higgs mass of about 125 GeV with relatively small $\tan\beta$, large A_t and a light stop, which is consistent with the current supersymmetric searches at the LHC.

Altogether then, these findings point to the fact that the CPV-MSSM provides an equally competitive solution (like its CPC counterpart) to the updated LHC Higgs data, in fact offering very little in the way of distinction between these two SUSY models (CPC-MSSM and CPV-MSSM) at the current LHC run. Improvement in different Higgs coupling measurements is necessary in order to test the possibility of probing the mild dependence of these CPV phases in the Higgs sector of the minimal SUSY realization.

Acknowledgments

A.C. would like to acknowledge the hospitality provided by IIT Guwahati where part of this work was done. J.L.D.-C. acknowledges support from VIEP-BUAP and CONACYT-SNI (Mexico). The work of S.M. is supported in part through the NExT Institute. The work of P.P. and B.D. is supported by a SERC, DST (India) project, SR/S2/HEP-41/2009. A.C. would like to thank Dr. Debottam Das and Dr. Biplob Bhattacharjee for useful discussions.

References

- [1] CMS Collaboration, Phys. Lett. B **716**, 30 (2012).
- [2] ATLAS Collaboration, Phys. Lett. B **716**, 1 (2012).
- [3] S. Chatrchyan *et al.* [CMS Collaboration], JHEP **1306**, 081 (2013).
- [4] ATLAS Collaboration: ATLAS-CONF-2013-014.

- [5] CMS Collaboration, CMS-PAS-HIG-13-001.
- [6] CMS Collaboration, CMS-PAS-HIG-13-002.
- [7] CMS Collaboration, CMS-PAS-HIG-13-003.
- [8] CMS Collaboration, CMS-PAS-HIG-13-004.
- [9] CMS Collaboration, CMS-PAS HIG-13-012.
- [10] CMS Collaboration, CMS-PAS-HIG-13-005.
- [11] ATLAS Collaboration, ATLAS-CONF-2013-012.
- [12] ATLAS Collaboration, ATLAS-CONF-2013-013.
- [13] ATLAS Collaboration, ATLAS-CONF-2013-030.
- [14] ATLAS Collaboration, ATLAS-CONF-2013-079.
- [15] ATLAS Collaboration, ATLAS-CONF-2012-160.
- [16] ATLAS Collaboration, ATLAS-CONF-2013-014.
- [17] ATLAS Collaboration, ATLAS-CONF-2014-009.
- [18] For reviews on Supersymmetry, see, J. Wess and J. Bagger, *Supersymmetry and Supergravity*, 2nd ed. (Princeton University Press, Princeton, 1991); M. Drees, P. Roy and R. M. Godbole, *Theory and Phenomenology of Sparticles*, (World Scientific, Singapore, 2005); H. E. Haber and G. Kane, Phys. Rep. **117**, 75 (1985); H. P. Nilles, Phys. Rep. **110**, 1 (1984).
- [19] S. P. Martin, hep-ph/9709356.
- [20] A. Djouadi, Phys. Rept. **457**, 1 (2008).
- [21] A. Djouadi, Phys. Rept. **459**, 1 (2008).
- [22] A. Arbey, M. Battaglia, A. Djouadi, F. Mahmoudi, Phys. Lett. B **720**, 153 (2013).
- [23] P. Bechtle, S. Heinemeyer, O. Stal, T. Stefaniak, G. Weiglein and L. Zeune, arXiv:1211.1955.
- [24] K. Schmidt-Hoberg, F. Staub and M. W. Winkler, JHEP **1301**, 124 (2013).
- [25] Z. Heng, arXiv:1210.3751.
- [26] M. Drees, Phys. Rev. D **86**, 115018 (2012).
- [27] A. Arbey, M. Battaglia, A. Djouadi, F. Mahmoudi, JHEP **1209**, 107 (2012).

- [28] K. Schmidt-Hoberg and F. Staub, JHEP **1210**, 195 (2012).
- [29] M. Carena, I. Low, C. E. M. Wagner, JHEP **1208**, 060 (2012).
- [30] M. Carena, S. Gori, N. R. Shah, C. E. M. Wagner, JHEP **1203**, 014 (2012).
- [31] L. J. Hall, D. Pinner, J. T. Ruderman, JHEP **1204**, 131 (2012).
- [32] S. Heinemeyer, O. Stal, G. Weiglein, Phys. Lett. B **710**, 201 (2012).
- [33] A. Arbey, M. Battaglia, A. Djouadi, F. Mahmoudi, J. Quevillon, Phys. Lett. B **708**, 162 (2012).
- [34] P. Draper, P. Meade, M. Reece, D. Shih, Phys. Rev. D **85**, 095007 (2012).
- [35] N. Chen, H. -J. He, JHEP **1204**, 062 (2012).
- [36] G. Guo, B. Ren, X. -G. He, arXiv:1112.3188.
- [37] X. -G. He, B. Ren, J. Tandean Phys. Rev. D **85**, 093019 (2012).
- [38] A. Djouadi, O. Lebedev, Y. Mambrini, J. Quevillon, Phys. Lett. B **709**, 65 (2012).
- [39] K. Cheung, T. -C. Yuan, Phys. Rev. Lett. **108**, 141602 (2012).
- [40] M. Hameda, S. Khalil and S. Moretti, Phys. Rev. D **89**, 011701 (2014).
- [41] A. Belyaev, S. Khalil, S. Moretti and M. Thomas, arXiv:1312.1935 [hep-ph].
- [42] B. Batell, S. Gori, L. -T. Wang, JHEP **1206**, 172 (2012).
- [43] M. Kadastik, K. Kannike, A. Racioppi, M. Raidal, JHEP **1205**, 061 (2012); H. Baer, V. Barger, A. Mustafayev, Phys. Rev. D **85**, 075010 (2012); J. F. Gunion, Y. Jiang, S. Kraml, Phys. Lett. B **710**, 454 (2012); L. Aparicio, D. G. Cerdeno, L. E. Ibanez, JHEP **1204**, 126 (2012); J. Ellis, K. A. Olive, Eur. Phys. J. C **72**, 2005 (2012); H. Baer, V. Barger, A. Mustafayev, JHEP **1205**, 091 (2012); N. Desai, B. Mukhopadhyaya, S. Niyogi, arXiv:1202.5190 J. Cao, Z. Heng, D. Li, J. M. Yang, Phys. Lett. B **710**, 665 (2012).
- [44] S. F. King, M. Muhlleitner, R. Nevzorov, K. Walz, Nucl. Phys. B **870**, 323 (2013); J. F. Gunion, Y. Jiang, S. Kraml, Phys. Rev. D **86**, 071702 (2012); G. Belanger, U. Ellwanger, J. F. Gunion, Y. Jiang, S. Kraml, J. H. Schwarz, JHEP **1301**, 069 (2013); J. F. Gunion, Y. Jiang, S. Kraml, Phys. Lett. B **710**, 454 (2012); U. Ellwanger, C. Hugonie, Adv. High Energy Phys. **2012**, 625389 (2012); U. Ellwanger, JHEP **1203**, 044 (2012); J. -J. Cao, Z. -X. Heng, J. M. Yang, Y. -M. Zhang, J. -Y. Zhu, JHEP **1203**, 086 (2012); Z. Kang, J. Li and T. Li, JHEP **1211**, 024 (2012).

- [45] A. Elsayed, S. Khalil and S. Moretti, Phys. Lett. B **715**, 208 (2012); L. Basso and F. Staub, arXiv:1210.7946 [hep-ph].
- [46] A. Dedes and S. Moretti, Nucl. Phys. B **576**, 29 (2000).
- [47] A. Dedes and S. Moretti, Phys. Rev. Lett. **84**, 22 (2000).
- [48] S. Hesselbach, S. Moretti, S. Munir and P. Poulose, J. Phys. Conf. Ser. **335**, 012020 (2011).
- [49] S. Hesselbach, S. Moretti, S. Munir and P. Poulose, AIP Conf. Proc. **1200**, 498 (2010).
- [50] S. Moretti, S. Munir and P. Poulose, Phys. Lett. B **649**, 206 (2007).
- [51] S. Hesselbach, S. Moretti, S. Munir and P. Poulose, Eur. Phys. J. C **54**, 129 (2008).
- [52] S. Hesselbach, S. Moretti, S. Munir and P. Poulose, Phys. Rev. D **82**, 074004 (2010).
- [53] O. Kittel, hep-ph/0504183.
- [54] I. Hinchliffe and N. Kersting, Phys. Rev. D **63**, 015003 (2001).
- [55] S. W. Ham, S. G. Jo, S. K. OH and D. Son, arXiv:0711.3951 [hep-ph].
- [56] T. Gajdosik, R. M. Godbole and S. Kraml, JHEP **0409**, 051 (2004).
- [57] T. -F. Feng, X. -Q. Li and J. Maalampi, Phys. Rev. D **73**, 035011 (2006).
- [58] J. R. Ellis, J. S. Lee and A. Pilaftsis, Phys. Rev. D **70**, 075010 (2004).
- [59] S. Baek and P. Ko, Phys. Rev. Lett. **83**, 488 (1999).
- [60] W. Altmannshofer, A. J. Buras and P. Paradisi, Phys. Lett. B **669**, 239 (2008).
- [61] D. A. Demir, A. Masiero and O. Vives, Phys. Rev. D **61**, 075009 (2000).
- [62] D. A. Demir, Phys. Rev. D **60**, 055006 (1999).
- [63] S. Y. Choi and J. S. Lee, Phys. Rev. D **61**, 115002 (2000).
- [64] S. Y. Choi, K. Hagiwara and J. S. Lee, Phys. Lett. B **529**, 212 (2002).
- [65] G. L. Kane and L. -T. Wang, Phys. Lett. B **488**, 383 (2000).
- [66] M. S. Carena, J. R. Ellis, A. Pilaftsis and C. E. M. Wagner, Phys. Lett. B **495**, 155 (2000).
- [67] J. R. Ellis, J. S. Lee and A. Pilaftsis, Phys. Rev. D **72**, 095006 (2005).
- [68] R. M. Godbole, S. Kraml, S. D. Rindani and R. K. Singh, Phys. Rev. D **74**, 095006 (2006) [Erratum-ibid. D **74**, 119901 (2006)].

- [69] A. G. Akeroyd and A. Arhrib, Phys. Rev. D **64**, 095018 (2001).
- [70] S. Y. Choi, K. Hagiwara and J. S. Lee, Phys. Rev. D **64**, 032004 (2001).
- [71] S. Y. Choi, M. Drees, J. S. Lee and J. Song, Eur. Phys. J. C **25**, 307 (2002).
- [72] F. Deppisch and O. Kittel, JHEP **0909**, 110 (2009) [Erratum-ibid. **1003**, 091 (2010)].
- [73] D. K. Ghosh, R. M. Godbole and D. P. Roy, Phys. Lett. B **628**, 131 (2005).
- [74] D. K. Ghosh and S. Moretti, Eur. Phys. J. C **42**, 341 (2005).
- [75] A. Arhrib, D. K. Ghosh and O. C. W. Kong, Phys. Lett. B **537**, 217 (2002).
- [76] B. Bhattacharjee, A. Chakraborty, D. Kumar Ghosh and S. Raychaudhuri, Phys. Rev. D **86**, 075012 (2012).
- [77] A. Bartl, S. Hesselbach, K. Hidaka, T. Kernreiter and W. Porod, Phys. Rev. D **70**, 035003 (2004).
- [78] A. Bartl, S. Hesselbach, K. Hidaka, T. Kernreiter and W. Porod, hep-ph/0409347.
- [79] C. -H. Chen, Phys. Lett. B **579**, 371 (2004).
- [80] A. Bartl, S. Hesselbach, K. Hidaka, T. Kernreiter and W. Porod, Phys. Lett. B **573**, 153 (2003).
- [81] A. Bartl, S. Hesselbach, K. Hidaka, T. Kernreiter and W. Porod, hep-ph/0306281.
- [82] T. Ibrahim, U. Chattopadhyay and P. Nath, Phys. Rev. D **64**, 016010 (2001).
- [83] T. Ibrahim, Phys. Rev. D **64**, 035009 (2001).
- [84] T. Ibrahim and P. Nath, Phys. Rev. D **61**, 093004 (2000).
- [85] Y. Li, S. Profumo and M. Ramsey-Musolf, JHEP **1008**, 062 (2010).
- [86] A. Romanino and A. Strumia, Nucl. Phys. B **490**, 3 (1997).
- [87] L. Mercolli and C. Smith, Nucl. Phys. B **817**, 1 (2009).
- [88] S. Yaser Ayazi and Y. Farzan, Phys. Rev. D **74**, 055008 (2006).
- [89] H. Georgi, A. Pais, Phys. Rev. D **10** (1974) 1246; N. Maekawa, Phys. Lett. B **282**, 387 (1992); A. Pilaftsis, Phys. Lett. B **435**, 88 (1998).
- [90] O. C.W. Kong, F. L. Lin, Phys. Lett. B **418**, 217 (1998); N. Haba, Phys. Lett. B **398**, 305 (1997); A. Pomarol, Phys. Lett. B **287**, 331 (1992).

- [91] A. Pilaftsis and C. E. M. Wagner, Nucl. Phys. B **553**, 3 (1999).
- [92] M. S. Carena, J. R. Espinosa, M. Quiros and C. E. M. Wagner, Phys. Lett. B **355**, 209 (1995).
- [93] A. Pilaftsis, Phys. Rev. D **58**, 096010 (1998).
- [94] S. Y. Choi, M. Drees and J. S. Lee, Phys. Lett. B **481**, 57 (2000).
- [95] S. Y. Choi, J. Kalinowski, Y. Liao and P. M. Zerwas, Eur. Phys. J. C **40**, 555 (2005).
- [96] M. S. Carena, J. R. Ellis, A. Pilaftsis and C. E. M. Wagner, Nucl. Phys. B **625**, 345 (2002).
- [97] M. S. Carena, J. R. Ellis, A. Pilaftsis and C. E. M. Wagner, Nucl. Phys. B **586**, 92 (2000).
- [98] K. E. Williams, H. Rzehak and G. Weiglein, Eur. Phys. J. C **71**, 1669 (2011).
- [99] M. Frank, T. Hahn, S. Heinemeyer, W. Hollik, H. Rzehak and G. Weiglein, JHEP **0702**, 047 (2007).
- [100] D. Chang, W. -Y. Keung and A. Pilaftsis, Phys. Rev. Lett. **82**, 900 (1999) [Erratum-ibid. **83**, 3972 (1999)].
- [101] A. Pilaftsis, Nucl. Phys. B **644**, 263 (2002).
- [102] K. A. Olive, M. Pospelov, A. Ritz and Y. Santoso, Phys. Rev. D **72**, 075001 (2005).
- [103] W. C. Griffith, M. D. Swallows, T. H. Loftus, M. V. Romalis, B. R. Heckel and E. N. Fortson, Phys. Rev. Lett. **102**, 101601 (2009).
- [104] J. J. Hudson, D. M. Kara, I. J. Smallman, B. E. Sauer, M. R. Tarbutt and E. A. Hinds, Nature **473**, 493 (2011).
- [105] B. C. Regan, E. D. Commins, C. J. Schmidt and D. DeMille, Phys. Rev. Lett. **88**, 071805 (2002).
- [106] M. Jung, JHEP **1305**, 168 (2013).
- [107] J. Baron *et al.* [ACME Collaboration], arXiv:1310.7534 [physics.atom-ph].
- [108] M. Jung and A. Pich, arXiv:1308.6283 [hep-ph].
- [109] A. P. Serebrov, E. A. Kolomenskiy, A. N. Pirozhkov, I. A. Krasnosheikova, A. V. Vasiliev, A. O. Polyushkin, M. S. Lasakov and A. K. Fomin *et al.*, arXiv:1310.5588 [nucl-ex].
- [110] C. A. Baker, D. D. Doyle, P. Geltenbort, K. Green, M. G. D. van der Grinten, P. G. Harris, P. Iaydjiev and S. N. Ivanov *et al.*, Phys. Rev. Lett. **97**, 131801 (2006).
- [111] J. Ellis, J. S. Lee and A. Pilaftsis, JHEP **1102**, 045 (2011).

- [112] L. I. Schiff, Phys. Rev. **132**, 2194 (1963).
- [113] J. Engel, M. J. Ramsey-Musolf and U. van Kolck, Prog. Part. Nucl. Phys. **71**, 21 (2013).
- [114] A. Sopczak [ALEPH and DELPHI and L3 and OPAL Collaborations], hep-ph/0602136.
- [115] S. Schael *et al.* [ALEPH and DELPHI and L3 and OPAL and LEP Working Group for Higgs Boson Searches Collaborations], Eur. Phys. J. C **47**, 547 (2006).
- [116] J. Beringer *et al.* (Particle Data Group), Phys. Rev. D **86**, 010001 (2012).
- [117] A. J. Buras, J. Girrbach, D. Guadagnoli and G. Isidori, Eur. Phys. J. C **72**, 2172 (2012).
- [118] K. S. Babu and C. F. Kolda, Phys. Rev. Lett. **84**, 228 (2000).
- [119] S. R. Choudhury and N. Gaur, Phys. Lett. B **451**, 86 (1999).
- [120] W. Altmannshofer, M. Carena, N. R. Shah and F. Yu, JHEP **1301**, 160 (2013).
- [121] The ATLAS collaboration, ATLAS-CONF-2013-090.
- [122] CMS Collaboration [CMS Collaboration], CMS-PAS-HIG-13-021.
- [123] CMS and LHCb Collaborations [CMS and LHCb Collaboration], CMS-PAS-BPH-13-007.
- [124] R. Aaij *et al.* [LHCb Collaboration], Phys. Rev. Lett. **111**, 101805 (2013).
- [125] S. Chatrchyan *et al.* [CMS Collaboration], Phys. Rev. Lett. **111**, 101804 (2013).
- [126] S. Bertolini, F. Borzumati and A. Masiero, Phys. Rev. Lett. **59**, 180 (1987); N. G. Deshpande, P. Lo, J. Trampetic, G. Eilam and P. Singer, Phys. Rev. Lett. **59**, 183 (1987); B. Grinstein and M. B. Wise, Phys. Lett. B **201**, 274 (1988); B. Grinstein, R. P. Springer and M. B. Wise, Phys. Lett. B **202**, 138 (1988); W. -S. Hou and R. S. Willey, Phys. Lett. B **202**, 591 (1988); B. Grinstein, R. P. Springer and M. B. Wise, Nucl. Phys. B **339**, 269 (1990).
- [127] S. Bertolini, F. Borzumati, A. Masiero and G. Ridolfi, Nucl. Phys. B **353**, 591 (1991); R. Barbieri and G. F. Giudice, Phys. Lett. B **309**, 86 (1993); R. Garisto and J. N. Ng, Phys. Lett. B **315**, 372 (1993); P. Nath and R. L. Arnowitt, Phys. Lett. B **336**, 395 (1994); M. Ciuchini, G. Degrossi, P. Gambino and G. F. Giudice, Nucl. Phys. B **534**, 3 (1998).
- [128] M. S. Carena, D. Garcia, U. Nierste and C. E. M. Wagner, Phys. Lett. B **499**, 141 (2001).
- [129] Y. Amhis *et al.* [Heavy Flavor Averaging Group Collaboration].
- [130] A. J. Buras, P. H. Chankowski, J. Rosiek and L. Slawianowska, Nucl. Phys. B **659**, 3 (2003).
- [131] P. Ball and R. Fleischer, Eur. Phys. J. C **48**, 413 (2006).

- [132] G. Isidori and F. Teubert, *Eur. Phys. J. Plus* **129**, 40 (2014).
- [133] M. Bona *et al.* [UTfit Collaboration], *JHEP* **0610**, 081 (2006).
- [134] RAaij *et al.* [LHCb Collaboration], *New J. Phys.* **15**, 053021 (2013).
- [135] A. Lenz and U. Nierste, arXiv:1102.4274 [hep-ph].
- [136] G. Isidori and P. Paradisi, *Phys. Lett. B* **639**, 499 (2006).
- [137] N. Fornengo, S. Scopel and A. Bottino, *Phys. Rev. D* **83**, 015001 (2011).
- [138] M. Chakraborti, U. Chattopadhyay and R. M. Godbole, *Phys. Rev. D* **87**, no. 3, 035022 (2013).
- [139] J. S. Lee, M. Carena, J. Ellis, A. Pilaftsis and C. E. M. Wagner, *Comput. Phys. Commun.* **184**, 1220 (2013); J. S. Lee, M. Carena, J. Ellis, A. Pilaftsis and C. E. M. Wagner, *Comput. Phys. Commun.* **180**, 312 (2009); J. S. Lee, A. Pilaftsis, M. S. Carena, S. Y. Choi, M. Drees, J. R. Ellis and C. E. M. Wagner, *Comput. Phys. Commun.* **156**, 283 (2004).
- [140] CMS Collaboration CMS-PAS-SUS-12-005, CMS-PAS-SUS-13-012.
- [141] ATLAS Collaboration ATLAS-CONF-2012-109, ATLAS-CONF-2013-047, ATLAS-CONF-2013-062.
- [142] G. Aad *et al.* [ATLAS Collaboration], *JHEP* **1302**, 095 (2013).
- [143] K. Hagiwara, J. S. Lee and J. Nakamura, *JHEP* **1210**, 002 (2012).
- [144] M. Carena, S. Gori, N. R. Shah, C. E. M. Wagner and L. -T. Wang, *JHEP* **1308**, 087 (2013).
- [145] G. Aad *et al.* [ATLAS Collaboration], *Phys. Lett. B* **726**, 88 (2013)
- [146] S. Chatrchyan *et al.* [CMS Collaboration], *Phys. Rev. D* **89**, 092007 (2014)
- [147] A. Freitas and P. Schwaller, *Phys. Rev. D* **87**, no. 5, 055014 (2013)
- [148] G. Belanger, B. Dumont, U. Ellwanger, J. F. Gunion and S. Kraml, *JHEP* **1302**, 053 (2013)
- [149] K. Cheung, J. S. Lee and P. Y. Tseng, *JHEP* **1305**, 134 (2013)
- [150] K. Cheung, J. S. Lee and P. Y. Tseng, arXiv:1407.8236 [hep-ph].
- [151] K. Cheung, J. S. Lee, E. Senaha and P. Y. Tseng, *JHEP* **1406**, 149 (2014)
- [152] M. J. Dolan, P. Harris, M. Jankowiak and M. Spannowsky, arXiv:1406.3322 [hep-ph].
- [153] J. Shu and Y. Zhang, *Phys. Rev. Lett.* **111**, no. 9, 091801 (2013)